White Rose Research Online

eprints@whiterose.ac.uk
https://eprints.whiterose.ac.uk
Universities of Leeds, Sheffield and York

Deposited via The University of Leeds.

White Rose Research Online URL for this paper:
https://eprints.whiterose.ac.uk/id/eprint/104272/

Version: Accepted Version

Article:
Schumann, S, Jackson, BR, Yule, I et al. (2016) Targeting the ATP-dependent formation of herpesvirus ribonucleoprotein particle assembly as an antiviral approach. Nature Microbiology, 2. 16201.

https://doi.org/10.1038/nmicrobiol.2016.201

(c) 2016, Macmillan Publishers Limited, part of Springer Nature. All rights reserved. This is an author produced version of a paper published in Nature Microbiology. Uploaded in accordance with the publisher's self-archiving policy.

Reuse
Items deposited in White Rose Research Online are protected by copyright, with all rights reserved unless indicated otherwise. They may be downloaded and/or printed for private study, or other acts as permitted by national copyright laws. The publisher or other rights holders may allow further reproduction and re-use of the full text version. This is indicated by the licence information on the White Rose Research Online record for the item.

Takedown
If you consider content in White Rose Research Online to be in breach of UK law, please notify us by emailing eprints@whiterose.ac.uk including the URL of the record and the reason for the withdrawal request.

UNIVERSITY OF LEEDS
University of Sheffield
UNIVERSITY of York

Targeting the ATP-dependent formation of herpesvirus ribonucleoprotein particle assembly as an antiviral approach

Sophie Schumann[1,2], Brian R. Jackson[1,2], Ian Yule[3], Steven K. Whitehead[3], Charlotte Revill[3], Richard Foster[2,3,*] and Adrian Whitehouse[1,2,*]

[1]School of Molecular and Cellular Biology, [2]Astbury Centre for Structural Molecular Biology, [3]School of Chemistry, University of Leeds, Leeds, LS2 9JT, United Kingdom.

*Correspondence to Adrian Whitehouse and Richard Foster
Tel: +44 (0)113-343-7096; +44 (0)113-343-5759
Email: a.whitehouse@leeds.ac.uk; r.foster@leeds.ac.uk

No of pages: 31
No of figures: 5
No of tables: 1
No of supplementary figures: 14
Abstract word count: 135
Main Text word count: 3446 words

Running Title: KSHV ORF57-hTREX inhibition

ABSTRACT

Human herpesviruses are responsible for a range of debilitating acute and recurrent diseases, including a number of malignancies. Current treatments are limited to targeting the herpesvirus DNA polymerases, however with emerging viral resistance and little efficacy against the oncogenic herpesviruses, there is an urgent need for new antiviral strategies. Herein we describe a mechanism to inhibit the replication of the oncogenic herpesvirus Kaposi's sarcoma associated herpesvirus (KSHV), by targeting the ATP-dependent formation of viral ribonucleoprotein particles (vRNPs). We demonstrate that small molecule inhibitors which selectively inhibit the ATPase activity of the cellular human transcription/export complex (hTREX) protein UAP56, result in effective inhibition of vRNP formation, viral lytic replication and infectious virion production. Strikingly, as all human herpesviruses utilize conserved mRNA processing pathways involving hTREX components, we demonstrate the feasibility of this approach for pan-herpesvirus inhibition.

Human herpesviruses are responsible for a range of acute and chronic diseases, including several cancers[1-3]. Kaposi's sarcoma-associated herpesvirus (KSHV) is the etiologic agent of Kaposi's sarcoma and two lymphoproliferative disorders; primary effusion lymphoma and multicentric Castleman's disease[4]. Like all herpesviruses, KSHV has two distinct forms of infection; latency and lytic replication. While the majority of KSHV-associated tumorigenic cells harbor latent virus, lytic gene expression occurs to various levels in each KSHV-associated disorder[5-11], suggesting that lytic replication inhibition may provide therapeutic intervention. Currently, drugs in clinical use are inhibitors of herpesvirus DNA polymerases. These nucleotide, nucleoside and pyrophosphate analogues are highly effective against a variety of herpesviruses, although drug-resistant strains can emerge in immunocompromised patients, carrying mutations in genes encoding the thymidine kinase, protein kinase or DNA polymerase[12]. Moreover, varying efficacy has been reported against the oncogenic gamma-herpesvirus subfamily[13-17]. Consequently, there is an urgent need for the continued development of anti-herpesvirus drugs, particularly targeting oncogenic herpesviruses.

RNA helicases contribute to remodeling of intramolecular RNA-, RNA-protein and protein-protein interactions in an ATP-dependent manner[18]. Both viral and cellular RNA helicases have central roles in virus life cycles and have emerged as therapeutic targets[19]. Numerous studies have evaluated the potential of targeting virally-encoded RNA helicases[20-22]. However, to circumvent viral resistance, inhibiting cellular RNA helicases has also been explored, supported by efforts targeting eIF4A for the treatment of cancer and DDX3 to inhibit HIV replication, illustrating selective pharmacological targeting of RNA helicases is possible[23-25].

The KSHV open reading frame (ORF) 57 protein, which has a functional homologue in each human herpesvirus, is essential for viral lytic replication[26]. It is a multifunctional protein involved in all stages of viral mRNA processing via an interaction with the human transcription/export (hTREX) complex[27]. hTREX is a large multiprotein complex involved in Nxf1-mediated cellular bulk mRNA nuclear export. Notably, ORF57-mediated hTREX recruitment produces a viral ribonucleoprotein particle (vRNP) essential for KSHV lytic replication[28,29]. ORF57 forms a direct interaction with the cellular export adapter Aly, however, redundancy in the cellular mRNA export pathway also allows ORF57 to facilitate vRNP formation via an interaction with UIF[29,30]. As such, disrupting the ORF57-hTREX interaction requires blocking multiple protein-protein interactions. Alternatively, the cellular RNA-helicase UAP56 functions as an essential hTREX assembly factor, forming an ATP-dependent trimeric complex with Aly and CIP29, as well as recruiting further hTREX components onto mRNAs[31,32]. Therefore, we examined the potential of inhibiting UAP56 ATPase activity, to prevent KSHV vRNP formation and lytic replication. *In silico* high-throughput screening

identified small molecules capable of binding the UAP56 ATP-binding pocket. Strikingly, results demonstrate that inhibiting UAP56 ATPase activity represents an antiviral target.

RESULTS

KSHV vRNP formation is ATP-cycle dependent

KSHV ORF57 interacts with hTREX to form an export-competent vRNP[33]. As the hTREX core component, UAP56, has RNA-stimulated ATPase activity, we assessed whether ATP binding/hydrolysis are required for ORF57-mediated vRNP formation. Co-immunoprecipitation assays were performed using lysates from HEK-293T cells transfected with GFP or GFP-UAP56 in the absence/presence of ORF57-mCherry, supplemented with 1.25 mM ATP or a non-hydrolysable ATP analogue, Adenosine 5'-O-(3-thio)triphosphate (ATPγS). Results showed that the ORF57-UAP56 interaction, hence vRNP formation, is ATP-dependent **(Fig. 1a)**. ATP enhanced the interaction between ORF57 and endogenous hTREX proteins. Conversely, ATPγS significantly inhibited the ORF57-UAP56 interaction, highlighting the necessity of ATP hydrolysis for vRNP formation. Notably, Aly and CIP29 binding with UAP56 was unaffected by ATPγS and a small, but significant increase in binding could be observed compared to controls **(Fig. 1b)**. The effect of ATP and ATPγS on the UAP56-ORF57 interaction was dose-dependent **(Supplementary Fig. 1a)**. Importantly, results suggest that inhibiting ATP hydrolysis prevents ORF57-mediated vRNP formation, without disrupting endogenous hTREX.

Since ORF57-hTREX binding is disrupted by ATPγS, we speculated that UAP56 ATPase function is required for hTREX remodeling, enabling ORF57 association. Either the energy-generating step of ATP hydrolysis or its product, ADP, binding to UAP56 was responsible for the conformational change allowing ORF57 binding. Co-immunoprecipitation assays performed in the presence of ADP disrupted the UAP56-ORF57 interaction in a dose dependent manner, indicating that ATP hydrolysis is the essential factor for the ORF57-hTREX interaction **(Fig. 1c, d; Supplementary Fig. 1b)**. However, ADP also disrupted endogenous hTREX. This data indicates an ATP-cycle dependent remodeling of hTREX enabling vRNP formation **(Fig. 1e)**. Upon ATP-binding endogenous hTREX is formed, ATP-hydrolysis then initiates a conformational change within hTREX allowing ORF57 binding. After release of inorganic phosphate, bound ADP causes complex dissociation.

Screening for UAP56 ATPase inhibitors

We speculated that inhibitors targeting UAP56 ATPase activity would prevent ORF57-mediated vRNP formation. Importantly, ATPγS-based experiments indicate a potential to prevent vRNP formation whilst maintaining endogenous hTREX. *In silico* high-throughput screening (HTS) was utilized to identify small-molecules capable of binding the UAP56 adenine-binding site, based on the UAP56:ADP co-crystal structure[34]. Favored compounds were tested for their potential to inhibit recombinant UAP56 ATPase activity. The most potent

compound, CCT018159 **(Fig. 2a)**, reduced UAP56 activity by >70% at 100 µM. Molecular modeling predicted CCT018159 binds the UAP56 ADP-binding pocket, with the resorcinol substructure mimicking the adenine unit of ADP and the methyl group at the 5-position of the pyrazole ring projecting towards the phosphate channel **(Fig. 2b-d)**. The molecule forms H-bonding interactions from the resorcinol hydroxyls to His67, Glu66 and Gln72 and a π-stacking interaction from the aryl ring to Phe65. The rest of the interactions are hydrophobic in nature (Met93, Gly92, Gly94 and Gly64). UAP56 inhibition was dose-dependent with non-linear regression determining a half maximal inhibitory concentration (IC_{50}) of 64.3 ± 2.5 µM (mean ± s.e.m.) **(Fig. 2e)**.

CCT018159 has previously been identified by HTS as a heat shock protein 90 (HSP90) inhibitor[35], we therefore calculated the inhibitory constant (K_i) comparing affinities towards UAP56 and HSP90, a value which takes enzyme and substrate concentrations utilized in biochemical assays into account. Employing the published K_M value for UAP56 ATP binding[36], we calculated a K_i value of 5.5 ± 0.2 µM for CCT018159, similar to the reported K_i of 1.8 ± 0.3 µM of CCT018159 against HSP90[37]. To examine the specificity of CCT018159 against UAP56, we utilized 17-DMAG, an alternative HSP90 inhibitor, but found no UAP56 ATPase inhibition **(Supplementary Fig. 2a)**. Microscale thermophoresis also confirmed CCT018159-UAP56 binding **(Fig. 2f, Supplementary Fig. 2b, c)**, yielding a K_D of 76.0 ± 3.8 µM, indicating relatively weak binding in a similar range to its natural substrate, ATP (K_D = 30.1 ± 4.5 µM). Finally, using an ADP-displacement assay, we confirmed that CTT018159 is an ATP/ADP-competitive inhibitor binding in the UAP56 adenine-binding pocket **(Fig. 2g)**. Notably, these assays used recombinant UAP56 in the absence of any cellular co-factors, apart from RNA, which may affect the CCT018159-UAP56 binding affinity, as shown for hTREX components stimulating UAP56 ATPase activity[32].

CCT018159 disrupts vRNP formation without inhibiting cellular mRNA export

The effect of CCT018159 on vRNP formation was assessed using co-immunoprecipitation assays. MTS assays identified non-cytotoxic concentrations in HEK-293T cells, < 15 µM **(Fig. 3a)**. Cells were transfected with GFP or ORF57-GFP, then incubated in the absence/presence of a concentration series of CCT018159. After 24 h, co-immunoprecipitations were performed using an UAP56-specific antibody, again in the absence/presence of CCT018159. CCT018159 effectively reduced the ORF57-UAP56 interaction at 2.5 and 5 µM concentrations, whilst maintaining endogenous hTREX formation **(Fig. 3b, Supplementary Fig. 3a)**. Furthermore, up to 0.5 mM CCT018159 added to the lysate did not inhibit the hTREX-UAP56 interaction. To confirm UAP56-specific inhibition, co-immunoprecipitations were repeated in absence/presence of a concentration range of 17-DMAG showing minimal cytotoxicity **(Supplementary Fig. 3b, c)**. Encouragingly, the

ORF57-UAP56 interaction was not disrupted, indicating that CCT018159-mediated vRNP disruption is due to UAP56 inhibition. Additionally, ORF57-mediated nucleolar redistribution of hTREX components was also assessed[38]. CIP29 localizes to the nuclear speckles excluding the nucleolus, however, upon ORF57 expression CIP29 is redistributed and co-localizes with nucleolar ORF57[39]. Conversely in CCT018159-treated cells, ORF57 failed to redistribute CIP29 to the nucleolus, with both proteins localizing independently in the nuclear speckles **(Supplementary Fig. 3d)**.

Following effective vRNP disruption *in vitro* and in cell culture, we examined the effect of CCT018159 on ORF57-mediated mRNA processing. Cells were transfected with GFP or ORF57-GFP and a viral intronless ORF47 mRNA reporter construct, then treated with DMSO or CCT018159 for 18 h and ORF47 mRNA levels assessed in whole cell and cytoplasmic lysates **(Fig. 3c)**. The ORF57-hTREX interaction stabilizes viral mRNAs allowing enhanced viral mRNA export[40], and results confirmed an increase in whole cell and cytoplasmic ORF47 mRNA abundance. In contrast, CCT018159 abolished both stabilization and ORF47 mRNA export, with no significant difference over GFP-transfected controls. Together, data suggest that CCT018159 prevents the vRNP formation and downstream mRNA processing.

ORF57-hTREX binding results in a block of cellular bulk mRNA nuclear export[11]. Therefore, if CCT018159 disrupts ORF57-mediated vRNP formation without affecting endogenous hTREX, cellular bulk mRNA export should be restored. Fluorescence *in situ* hybridization (FISH) was used to monitor cellular bulk mRNA export **(Fig. 3d)**. In GFP-expressing cells, the majority of polyadenylated RNA (poly(A)-RNA) was detected in the cytoplasm with minor amounts in nuclear speckles. However, ORF57-mediated hTREX sequestration led to a marked reduction of cytoplasmic poly(A)-RNA and retention in the nucleus. Strikingly, in ORF57-expressing cells treated with CCT018159, nuclear retention was lost, with poly(A)-RNA present in the cytoplasm. Quantification of the FISH analysis showed this effect to be significant **(Fig. 3e)**. Importantly, results demonstrated that CCT018159 does not affect endogenous hTREX. Results were confirmed by qRT-PCR analysis, measuring the export of selected cellular mRNAs in the absence/presence of CCT018159 **(Supplementary Fig. 3e)**. FISH analysis was repeated in the presence of 17-DMAG, which failed to relieve ORF57-mediated nuclear retention of cellular bulk mRNA **(Supplementary Fig. 3f, g)**. This confirms CCT018159-mediated UAP56 inhibition independent of HSP90.

CCT018159 prevents KSHV lytic replication

ORF57-mediated vRNP formation is essential for KSHV lytic replication[33]. Therefore, we examined the potential of CCT018159 to inhibit KSHV replication using the KSHV-infected cell line TREx BCBL1-Rta[41]. MTS assays and non-linear regression determined the cytotoxic concentration 50 (CC_{50}) for 24 and 72 h time points **(Fig. 4a, b)**. Furthermore, no increase in

apoptosis was observed at 2.5 μM CCT018159 **(Supplementary Fig. 4a)**, contrary to the observed effect of HSP90 inhibitors in KSHV-infected cell lines[42,43]. TREx BCBL1-Rta cells remained latent or were reactivated with doxycycline and treated with increasing amounts of CCT018159. Immunoblotting using Myc and ORF57-specific antibodies (markers for induction of lytic replication) or the KSHV minor capsid protein (mCP)-specific antibody (viral lytic late protein dependent on vRNP assembly) showed a marked reduction in mCP expression at 2.5 μM CCT018159 **(Fig. 4c; Supplementary Fig. 4b)**, whereas no decrease in ORF57 expression is noted, confirming the decrease in mCP expression is not due to loss of ORF57 or lower reactivation levels **(Supplementary Figure 4b, c)**. Moreover, ORF57 is translated from an intron-containing transcript, indicating functional hTREX. Quantification and non-linear regression of mCP levels obtained an effective concentration 50 (EC_{50}) for viral protein expression. Importantly, the EC_{50} of 0.6 μM is far lower than the CC_{50} of 21 μM at this time point. A large "therapeutic window" is observed, showing that cytotoxicity occurred at higher concentrations than inhibition of viral protein expression **(Fig. 4c)**.

To assess whether CCT018159 also decreased viral genome replication and virion production, uninduced or reactivated TREx BCBL1-Rta cells were treated with increasing amounts of CCT018159 and qPCR used to determine viral load. A steep decrease in viral load was visible at 1 and 2.5 μM CCT018159 **(Fig. 4d)**. Non-linear regression calculated an EC_{50} on viral replication of 1.1 μM. Again, when compared to the 72 h CC_{50} of 16.6 μM, a large "therapeutic window" was observed. This concentration range produced dramatic inhibition of viral replication without any cytotoxicity. To examine virion production, supernatants were used to re-infect naïve cells and qRT-PCR determined KSHV gene expression. Cells re-infected with supernatant from CCT018159-treated cells contained 80% less viral mRNA than controls **(Fig. 4e)**. Together results suggest that CCT018159 is effective at inhibiting KSHV lytic replication and virion production.

To confirm CCT018159-mediated inhibition of KSHV replication is due to vRNP disruption and not HSP90 inhibition, we performed MTS and viral load assays using 17-DMAG. While a therapeutic window was observed, CC_{50} of 4.3 ± 0.9 μM and EC_{50} of 0.04 ± 0.01 μM **(Supplementary Fig. 4d)**, we noticed irregularities for both assays. The metabolic activity, reflecting cell viability, was initially increased, before decreasing at higher concentrations. This 17-DMAG-induced cellular stress resulted in increased levels of apoptosis and necrosis **(Supplementary Fig. 4e)**. This was in contrast to CCT018159, but reflects published results showing HSP90 inhibitors cause apoptosis[43,44], via vFLIP degradation and subsequent downregulation of NF-κB signaling pathway[43,44]. Importantly, NF-κB signaling is significantly reduced in 17-DMAG-treated cells compared to CCT018159 **(Supplementary Fig. 4f)**. Moreover, a decrease in viral load upon 17-DMAG treatment not only indicated a block in lytic reactivation, but also viral episome loss via KSHV latent nuclear

antigen (LANA) degradation[42]. Immunoblotting showed enhanced LANA and CDC2 degradation in the presence of 17-DMAG **(Supplementary Fig. 4g)**, whereas no LANA degradation was observed for a range of concentrations of CCT018159, although CDC2 levels were reduced from 5 µM. Notably, KSHV mCP inhibition occurred at concentrations of 1–2.5 µM CCT018159 **(Supplementary Fig. 5a-c)**. This data confirms that CCT018159-mediated inhibition is due to vRNP disruption, not HSP90-related inhibitory mechanisms.

Effect of CCT018159 structural analogues on KSHV replication

To assess a structure-activity-relationship, 4 structural analogues of CCT018159 were analyzed **(Table 1; Supplementary Fig. 6-9)**. An IC_{50} was determined for all analogues against recombinant UAP56 *in vitro*. The CC_{50} on TREx BCBL1-Rta cells was assessed by MTS assay and the inhibitory potential (EC_{50}) on viral protein production and genome load also determined. Furthermore, immunoprecipitations were employed to test those compounds effective against KSHV lytic replication for their ability to disrupt the UAP56-ORF57 interaction **(Supplementary Fig. 6f, 7f, 8f)**. All analogues present minor structural variations on CCT018159 at the 2,4-hydroxyphenyl, benzodioxanyl and pyrazole subsites. Removal of the ethyl group at the resorcinol substructure (Compound 2) was not detrimental to activity and showed similar inhibitory effects on KSHV replication, consistent with molecular modelling in which the ethyl group extends into solvent **(Fig. 2d)**. Replacement of the methyl group at the 5-position of the pyrazole ring with a carboxylic acid (Compound 4) ablated any inhibitory activity, suggesting the carboxylate group is not tolerated at the entrance to the phosphate channel, possibly due to its charged nature and relative proximity to two carbonyl groups (Gly-92, Thr-96) inducing a repulsive interaction. Supportive of this hypothesis, re-docking of the compound failed to generate a binding pose. Replacement of the dioxanyl ring with a methoxy group (Compound 3) and H (Compound 1) demonstrated a modest reduction of ATPase activity and KSHV inhibition, consistent with molecular modeling demonstrating a reduced potential for hydrophobic contact to the side-chain of Met93. The analogues were also tested for HSP90 inhibition. Notably, combining results with virus inhibition, a larger therapeutic window was observed for Compound 1 **(Supplementary Fig. 10a-c)**. CDC2 expression was constant below 15 µM, whereas effective mCP inhibition occurred between 2.5–5 µM. Compound 2 showed a marked decrease in expression for both mCP and CDC2 at 2.5 µM, suggesting an efficient HSP90 inhibitor **(Supplementary Fig. 11a-c)**. Therefore distinct responses were observed for all compounds, with CCT018159 and Compound 1 showing specifically inhibition of virus replication by inhibiting UAP56.

CCT018159 inhibits α- and β-herpesvirus replication

All herpesviruses encode an ORF57 homologue which utilizes hTREX components for vRNP assembly. To examine any potential pan-herpesvirus activity, we assessed the inhibitory effect of CCT018159 on the α- and β-herpesviruses, HSV-1 and HCMV, respectively. First, immunoprecipitations of UAP56 were repeated in the presence of the ORF57 homologues, HSV-1 ICP27 and HCMV UL69 **(Fig. 5a, b)**. Notably, CCT018159 reduced the interaction of both viral proteins and hTREX to a similar level observed for ORF57. Further, a non-cytotoxic working concentration of CCT018159 in HFF cells was determined **(Fig. 5c, d)**, cells were then infected with HSV-1, prior to treatment with increasing amounts of CCT018159. Cells were directly imaged for HSV-mediated cell lysis **(Supplementary Fig. 12a)** or assessed using a plaque assay **(Fig. 5e)**. Strikingly, with CCT018159 increasing concentrations, cell lysis, plaque size and plaque number was dramatically decreased, demonstrating efficient inhibition of HSV-1 replication. Moreover, a marked reduction in virion production was observed after re-infection with the harvested supernatant and assessment by flow cytometry **(Fig. 5f; Supplementary Fig. 12b),** plaque assay **(Fig. 5g)** and immunoblotting of the lytic protein, ICP27 **(Supplementary Fig. 12c)**. 2.5 μM CCT018159 resulted in a 50% reduction in infected cells, with a 95% reduction observed at 5 μM CCT018159.

Inhibition of HCMV lytic replication was assessed after infection of HFF cells and treatment with CCT018159. Cells were directly imaged for HCMV-mediated cell lysis **(Supplementary Fig. 12d)** and re-infection levels were quantified by qPCR **(Fig. 5h)**. Excitingly, 1 μM CCT018159 was found to reduce HCMV virion production by 50%, with over 99% reduction at 2.5 μM. Importantly, a 90% reduction of infectious HSV-1 or HCMV virion production was determined at 2.5 or 5 μM CCT018159, where no inhibition of HSP90 occurred **(Supplementary Fig. 13a-c)**, providing a clear therapeutic window. Together, these results show that CCT018159 has pan-herpesvirus activity.

DISCUSSION

Disrupting the ORF57-hTREX interaction is an antiviral target, however, strategies to block this interaction are complicated by redundancy in the mammalian mRNA export system[29]. Consequently we targeted the ATP-cycle dependent remodeling of hTREX required for vRNP formation. The UAP56 ATP-binding site is situated in a cleft between two connected helicase domains[34,45], with ATP-binding believed to bring these domains closer, enabling a closed conformation. Therefore, we speculate that inhibiting ATP hydrolysis traps UAP56 in the ATP-bound state allowing hTREX formation, however, further remodeling is required to accommodate the ORF57 protein. Interestingly, ATP hydrolysis-induced conformational changes in DEAD-box helicases are essential during RNA unwinding[18] and members of the exon junction complex (EJC) stabilize the post-hydrolysis state of eIF4III, trapping the protein onto RNA[46]. As ATP hydrolysis and hTREX remodeling is also necessary for Aly loading onto mRNA[32], we hypothesize this remodeling enables ORF57 binding.

Molecular modelling predicts CCT018159 binds the UAP56 adenine-binding pocket, suggesting an ATP-competitive inhibitor. While CCT018159 was found to inhibit purified UAP56 and displace ADP with an IC_{50} of about 60 µM, its antiviral effect was detected at 30-fold higher potency (around 2 µM). As it has previously been shown that hTREX proteins Aly and CIP29 stimulate UAP56 ATP binding and hydrolysis[31], it is not surprising that the affinity of UAP56 for CCT018159 should also change in the presence of cellular co-factors. Although CCT018159 is a known HSP90 inhibitor[35], demonstrating complex pharmacokinetics, including relatively high metabolic turnover, its favorable selectivity profile against closely related ATPases and a panel of kinases[37,47] make it a useful starting point for lead compound development. Data conclusively shows CCT018159-mediated UAP56 inhibition, disruption of the ORF57-hTREX interaction and lytic replication, with a differing phenotype from the HSP90-inhibitor, 17-DMAG. Nonetheless, as CCT018159-mediated HSP90 inhibition occurred at higher concentrations, restricting the therapeutic window, CCT018159 should be seen as a proof-of-principle and starting point for the development of UAP56-specific antivirals. We have identified analogues which demonstrate altered HSP90 inhibition, an important selection criterion for lead-generation UAP56 inhibitors. Future work will explore potential enhanced potency via extension into the phosphate channel.

Targeting a cellular RNA helicase can be assumed to reduce the risk for virus resistance and theoretically provides pan-viral activity. Notably, all herpesviruses encode ORF57 homologues and hTREX interactions are essential for their replication[33,48,49]. Excitingly, CCT018159 prevents replication of all three herpesvirus subfamilies, indicating possible pan-herpesviral activity and may have wider utilization, as other important human pathogens co-opt UAP56 for viral mRNA processing[50].

All correspondence and requests for materials should be addressed to Adrian Whitehouse (a.whitehouse@leeds.ac.uk).

Acknowledgements

We are indebted to Professors Jae Jung (UCLA), Stacey Efstathiou and John Sinclair (Cambridge) for cell lines and recombinant viruses and to Professors Stuart Wilson (Sheffield), Robin Reed (Harvard) and Thomas Stamminger (Erlangen) for the kind gift of antibodies and plasmid constructs. We also thank Dr Iain Mainfield, Centre for Biomolecular Interactions, Faculty of Biological Sciences for helpful advice. This work was supported in part by the Wellcome Trust (093788/Z/10/Z); Worldwide Cancer Research (12-1045), BBSRC (BB/000306; BB/M006557) and CRUK (C12057/A19430).

Author contribution

S.S. designed and performed experiments, analyzed data and wrote the manuscript; B.R.J. performed experiments and analyzed data; I.Y. performed the virtual high-throughput screening and modelling; S.K.W. and C.R. synthesized tested compounds; R.F. and A.W. designed and performed experiments, analyzed data and wrote the manuscript.

METHODS

Virtual high-throughput screening. Identification of UAP56 ATPase inhibitors was performed using virtual high-throughput screening of a University of Leeds proprietary 250k library of small molecules selected from the ZINC database[51], based on high structural diversity, adherence to Lipinski criteria and absence of pan interference (PAIN) scaffolds. Docking routines were performed using eHiTS (SymBioSys Inc.) and AutoDock4 (Scripps Research Institute) based on the UAP56Δ9 MgADP complex (1XTJ). Prior to docking ADP, Mg and the water molecules were removed and the protein prepared using the default settings within the Protein Preparation Wizard within Maestro9.4 (Schrödinger). eHiTS was used to screen the 250k library using a clip file generated around the ATP binding site and highest speed docking (accuracy mode 1). The 5k compounds which demonstrated the best eHiTS score based on the default scoring function with the software were re-docked using AutoDock4. Favored compounds (400) were selected for screening based on the default AutoDock4 scoring function and visualized for quality of binding mode and for compliance with attractive physicochemical properties (Lipinski's rules) and availability.

ATPase assay and compound screening. For the UAP56 ATPase assay 2.5 μM purified GST-UAP56 and where applicable GST were incubated with 50 μM yeast tRNA, 35 μM ATP, 2 mM $MgCl_2$ and 50 mM KCl in 50 mM Tris/HCl (pH 7.6). During compound screening, inhibitors were added to give final concentrations of 100 μM. For IC_{50} measurements, compounds of varying concentrations were delivered in 0.5 μl DMSO (1% of total reaction volume). Reactions were incubated at 37°C for 30 min, before Kinase-Glo® Reagent (Promega) was added according to the manufacturer's instructions to quantify remaining ATP by luminescence. All replicates were of biological nature.

ADP displacement assay. To assess competitive binding of CCT018159 to UAP56, an ATPase assay (as described above) containing 5 μM UAP56-GST and 5 μM ATP was run for 30 mins, to ensure all UAP56 was bound to ADP. Using an ADP-Glo™ Kinase assay kit (Promega) following the manufacturer's instructions, any remaining ATP was depleted, before CCT018159 was added in increasing concentrations and the reaction mixture was incubated at 37°C for 30 mins. Using the kit's reagents, all free ADP was converted to ATP and quantified by luminescence. All replicates were of biological nature.

Viral mRNA export assay. HEK-293T cells were co-transfected with GFP or ORF57-GFP and ORF47 expression constructs before subcellular fractionation. Quantitative qRT-PCR was performed on isolated RNA. Levels of the reporter mRNA ORF47 were normalized to GAPDH

and used to quantify viral mRNA export. The method has been described previously[29,38]. All replicates were of biological nature.

Fluorescence *in situ* hybridization. HEK-293T cells were transfected with GFP or ORF57-GFP for 6 h and subsequently treated with DMSO, CCT018159 or 17-DMAG for 24 h. Polyadenylated RNA was detected in with an oligo dT(70) probe labeled at the 5' end with Alexa Fluor 546 NHS Ester. The method was performed as published previously[31]. Cells were visualized on a Zeiss LSM 700 laser scanning confocal microscope and images analyzed using Zen® 2011 (Zeiss).

Infectious KSHV virion production. TREx BCBL1-Rta cells were harvested 72 h after reactivation of viral lytic replication. Filtered tissue culture supernatants were used 1:1 to inoculate 1×10^6 HEK-293T cells. Infected cells were quantified at 24 h post-infection by real-time qRT-PCR. RNA was extracted from total cell lysates using TRIzol (Invitrogen) as described by the manufacturer. RNA was DNase treated using the Ambion® DNase-free™ DNA removal kit, as per the manufacturer's instructions, and RNA (1 µg) from each fraction was reverse transcribed with M-MuLV Reverse Transcriptase (New England Biolabs, Inc.), as per the manufacturer's instructions, using oligo(dT) primers (Sigma-Aldrich®). Obtained cDNA served as template for qPCR reactions using *ORF47*, *ORF57* and *GAPDH* specific primers as described before. Replicates were of biological nature, with each used for 2 technical repeats.

Plasmids and antibodies. pGST-UAP56, pEGFP-UAP56, pORF47, pORF57-EGFP and pORF57-mCherry have been described previously[30,31,33,52]. pEGFP-N1 expressing eGFP (Clontech) and pGEX-4T.1 expressing GST (GE Healthcare) are commercially available. Antibodies against Aly (11G5) (Sigma-Aldrich®), GAPDH (6C5) (Abcam®), GFP (JL-8) (Clontech), ORF57 (207.6) (Santa Cruz Biotech®), UAP56 (rabbit polyclonal) (Abcam®), CHTOP (rabbit polyclonal) (Bethyl Laboratories, Inc.), mCP (sheep polyclonal) (Exalpha Biological, Inc.), CDC2 (A17) (Abcam®), HSP90 (4F10) (Santa Cruz Biotech®), LANA (13B10) (Leica Biosystems) and ICP27 (vP-20) (Santa Cruz Biotech®) were obtained from the respective companies. CIP29 antibody was a kind gift from Stuart Wilson (University of Sheffield)[31]. In general, antibodies were used for western blot analysis at a concentration of 1:5000, ORF57, ICP27, HSP90 and mCP were used at a 1:1000 dilution, CIP29 was used at a 1:2500 dilution.

Cell culture and viruses. HEK-293T were purchased from the ATCC (American Type Culture Collection) and HFF were a kind gift of John Sinclair (University of Cambridge). Both cell lines

were cultured in Dulbecco's modified Eagle's medium with glutamine (DMEM, Lonza) supplemented with 10% foetal calf serum (FCS, Gibco®) and 1% penicillin-streptomycin (Gibco®). TREx BCBL1-Rta cells, a human B-cell lymphoma cell line latently infected with KSHV and modified to contain doxycycline (dox)-inducible myc-RTA, were a kind gift of Jae U. Jung (University of Southern California) (Nakamura et al, 2003). TREx BCBL1-Rta cells were grown in RPMI1640 growth medium with glutamine (Gibco®), supplemented with 10% foetal calf serum (FCS, Gibco®) and 1% penicillin-streptomycin (Gibco®). For virus reactivation, 0.8×10^6 cells TREx BCBL1-Rta cells were induced using 2 µg/ml doxycycline hyclate (Sigma-Aldrich®). Cells were harvested after 24 h for analysis of protein expression, while viral load and production of new infectious virions was assessed after 72 h. HCMV (Merlin) and HSV-1 virus (SC16) stocks were kindly provided by John Sinclair and Stacey Efstathiou (University of Cambridge). For each cell line a large bank of cell stocks were established that were used throughout the duration of the project. To reduce any impact of phenotypic drift, prokaryotic contamination and inadvertent cross contamination, cell cultures were discarded after 15 passages and new cultures established from the bank. Used cell lines were tested negative for Mycoplasma in 11/2014 and 01/2016.

Co-immunoprecipitation assays. 1×10^6 HEK-293T cells were co-transfected with 1 µg of the indicated plasmid DNA (GFP, GFP-UAP56, ORF57-mCherry, ORF57-GFP, ICP27-GFP or pUL69-GFP) using Lipofectamine® 2000 according to manufacturer's instructions (Invitrogen™). Where indicated, cells were treated with CCT018159 6 h after transfection. After 24 h, transfected cells were lysed on ice for 20 min using 1 ml modified RIPA buffer (50 mM Tris/HCl, 150 mM NaCl, 1% NP40-alternative; pH 7.6) with the addition of 1 µl/ml RNase A (Invitrogen™). Lysates were clarified for 10 min at 16,000×g and the supernatants were pre-cleared against protein A beads (Roche) for 2 h at 4°C with end-over-end mixing. For the precipitations, 1 ml of pre-cleared lysate was incubated with 15 µl pre-washed GFP-trap® affinity beads (ChromoTek®) and the indicated amounts of ATP, ADP (Sigma-Aldrich®) or ATPγS (Jena Bioscience) for 2.5 h at 4°C while end-over-end mixing. Alternatively, cell lysates were incubated with 5 µg polyclonal UAP56 antibody for 16 h at 4°C while end-over-end mixing, before addition of Protein A agarose beads (Roche) for another 2 h. Where indicated, small molecule inhibitors were added in DMSO or EtOH, yielding a total of 0.1% DMSO or 0.5% EtOH per immunoprecipitation, which was also supplemented in all control precipitations. Beads were washed 4 times in ice-cold modified RIPA buffer and proteins were eluted in Laemmli buffer before analysis by western blotting as previously described[53].

Immunoblotting. Western blots were performed as previously described[33]. Briefly, protein samples were run on 10-12% polyacrylamide gels and transferred to nitrocellulose Hybond™-

C (GE Healthcare) membranes via tank blotting. Membranes were blocked with TBS + 0.1% v/v Tween® 20 and 5% w/v dried skimmed milk powder. Membranes were probed with relevant primary and secondary HRP-conjugated IgG antibodies (Dako), treated with EZ-ECL (Geneflow), and exposed to Hyperfilm ECL™ (GE Healthcare).

Recombinant protein expression. Recombinant GST and GST-UAP56 were expressed in *E.coli* BL-21 at 30°C over night and purified as described previously[13,28,54]. Proteins were eluted from the beads using 50 mM Tris/HCl (pH 7.6) with 10 mM reduced Glutathione and then further purified by buffer exchange using PD midiTrap™ G-25 columns (GE Healthcare) and 50 mM Tris/HCl, 50 mM KCl, 2 mM $MgCl_2$; pH 7.6).

Microscale thermophoresis. Microscale thermophoresis (MST) was carried out on a Monolith NT.115 Microscale Thermophoresis device using standard treated capillaries (NanoTemper Technologies). Recombinant GST-UAP56 was labelled with FITC (Sigma-Aldrich®) according to the manufacturer's instructions. Labelling reagent was removed by buffer-exchange chromatography using Zeba™ Spin Desalting Columns following the manufacturer's instructions and eluted into 20 mM HEPES (pH 7.4) with 2 mM $MgCl_2$. The concentration of labelled protein was used between 100 and 500 nM by diluting labelled protein in 20 mM HEPES (pH 7.4) with 2 mM $MgCl_2$. LED power was used at 10-60%. All reactions were performed at 37°C. Equal amounts of labelled protein were titrated by CCT018159 diluted in DMSO and 20 mM HEPES (pH7.4) with 2 mM $MgCl_2$ in a 1:1 series dilution starting with 4.5 mM CCT018159, such that the final concentration of DMSO was 20% (v/v) in all capillaries. Curve fitting and K_D determination was performed using the NTanalysis software (NanoTemper Technologies) in the Thermophoresis mode. All replicates were of biological nature.

Cell viability assay. Cell viability was measured in HEK-293T, TREx BCBL1-Rta and HFF cells using an MTS-based CellTiter 96® AQ_{ueous} One Solution Cell Proliferation Assay (Promega), following the manufacturer's instructions. HEK-293T cells were seeded at a concentration of 0.5×10^6 cells/ml and HFF cells at 1×10^5 cells/ml, 24 h before treatment with small molecule inhibitors. TREx BCBL1-Rta cells were seeded at 1×10^6 cells/ml and treated immediately. The indicated inhibitor concentrations were delivered in DMSO (0.1% of total volume), which was also added to all control wells, and incubated for 24 or 72 h, before cell viability was assessed. All replicates were of biological nature.

Apoptosis assay. Apoptotic and necrotic cells were stained using the Annexin-V-FLUOS Staining Kit and protocol from Roche. In brief, TREx BCBL1-Rta cells were treated with

DMSO, CCT018159 or 17-DMAG for 72 h, before they were washed and incubated in a HEPES buffer containing Annexin-V-Fluorescein and propidium iodide to label apoptotic and necrotic cells. Cells were analyzed using a flow cytometer. All replicates were of biological nature.

Immunofluorecence. Cell fixation and staining was performed as previously described[55]. Briefly, HEK-293T cells were grown on sterilized glass coverslips treated with Poly-L-Lysine before being transfected. After 24 h cells were washed in PBS and fixed in PBS containing 4% (v/v) paraformaldehyde for 10 minutes, washed twice in PBS and permeabilized using PBS containing 1% Triton X-100 for 10 minutes. Coverslips were then incubated with appropriate primary and secondary antibodies for 1 hour each at 37°C before being mounted onto microscope slides using Vectashield® with DAPI. Slides were visualized on a Zeiss LSM 700 laser scanning confocal microscope and images analyzed using Zen® 2011 (Zeiss).

KSHV replication assay. To determine the viral-DNA load, TREx BCBL1-Rta cells were harvested 72 h after reactivation of viral lytic replication. Total DNA was isolated using the QIAamp DNA mini kit (QIAGEN) following the manufacturer's instructions and quantified by UV spectrophotometry. Quantification of viral DNA copy numbers was performed using a Rotor-Gene 6000 Real-Time PCR machine (QIAGEN). Amplification was performed in 20 µl reaction volumes with 40 ng template DNA using SensiMix™*Plus* SYBR qPCR reactions (Bioline), as per manufacturer's instructions, with a standard 3-step melt program (95°C for 15 seconds, 60°C for 30 seconds, 72°C for 20 seconds). Amplifications of the viral gene *ORF57* were carried out using the forward primer 5'-TGTCAGTGGTGGACCTGAC and reverse primer 5'-GTGGTCGTTGAGGGCAATG. The viral gene *ORF47* was amplified using the forward primer 5'-CGCGGTCGTTCGAAGATTGGG and reverse primer 5'-CGAGTCTGACTTCCGCTAACA. *GAPDH* was amplified using the forward primer 5'-GCCATAATCAAGCGTACTGG and reverse primer 5'-GCAGACAAATATTGCGGTGT. Quantitative analysis for viral DNA levels with *GAPDH* as internal control was carried out using the comparative CT method as previously described[38]. Replicates were of biological nature, with each used for 2 technical repeats.

Primary HSV-1 infection. A MOI of 0.001 was used for primary infection of 2×10^5 HFF with HSV-1. Following 1 h incubation of cells with virus, cells were washed twice with PBS, followed by addition of growth media (for analysis of infectious HSV-1 virion production) or plaque agar (for HSV-1 plaque assays of primary infection). Both growth media and plaque agar were supplemented with small molecule inhibitor concentrations or DMSO (at a final concentration of 0.1% DMSO in all wells).

Infectious HSV-1 virion production. After 72 h primary HSV-1 infection, cell supernatants were diluted 1:10-10,000 with new growth media and incubated on 2×10^5 naïve HFF cells. Re-infection was analyzed by plaque assay (below) or using flow cytometry. For the latter, cells were incubated with infectious virions from a primary infection for 24 h, fixed using PBS with 4% (v/v) paraformaldehyde and washed twice again with PBS. As a recombinant virus expressing GFP was used, all HSV-1-infected cells were quantified via fluorescence using the BD LSRFortessa flow cytometer (BD Biosciences) on the FITC channel. All replicates were of biological nature.

HSV-1 plaque assay. Plaque assays were performed after primary infection or re-infection of naïve HFF cells with HSV-1, as described above. After 1 h incubation of 2×10^5 HFF cells with HSV-1, cells were washed twice with PBS and overlaid with plaque agar (1:1 dilution of growth media with 2% (w/v) molten agarose, tempered to 37°C). Small molecule inhibitors were added to plaque agar during primary HSV-1 infections, re-infection for assessment of infectious HSV-1 virion production was performed without additional inhibitors. The agarose was removed after 96 h, cells washed once with PBS, fixed 10 min with 4% (v/v) paraformaldehyde and stained using 0.5% (w/v) crystal violet stain. Viral plaques were counted by eye. All replicates were of biological nature.

Primary HCMV infection. A MOI of 0.08 and 0.008 was used for primary infection of 2×10^5 HFF with HCMV. Following 1 h incubation of cells with virus, the growth media was supplemented with small molecule inhibitor concentrations or DMSO (at a final concentration of 0.1% DMSO in all wells).

Infectious HCMV virion production. After 168 h primary HCMV infection, HFF cell supernatants were diluted 1:10 and 1:100 (for initial infection with an MOI of 0.08) or 1:10 (for initial infection with an MOI of 0.008) with new growth media and incubated on 2×10^5 naïve HFF cells for 20 h. Re-infection rates were measured by quantitative qPCR. For this, total DNA was isolated using the QIAamp DNA mini kit (QIAGEN) following the manufacturer's instructions and quantified by UV spectrophotometry. Quantification of viral DNA copy numbers was performed using a Rotor-Gene 6000 Real-Time PCR machine (QIAGEN). Amplification was performed in 20 µl reaction volumes with 40 ng template DNA using SensiMix™*Plus* SYBR qPCR reactions (Bioline), as per manufacturer's instructions, with a standard 3-step melt program (95°C for 15 seconds, 60°C for 30 seconds, 72°C for 20 seconds). Amplifications of the viral gene *UL69* were carried out using the forward primer 5'-TCGGTGGGATGAATTTGGTC and reverse primer 5'-CATGATAGCGTACTGTCCCTTC.

GAPDH was amplified using the forward primer 5'-GCCATAATCAAGCGTACTGG and reverse primer 5'-GCAGACAAATATTGCGGTGT. Quantitative analysis for viral DNA levels with GAPDH as internal control was carried out using the comparative CT method as previously described[38]. Replicates were of biological nature, with samples from one concentration series used for a control technical repeat.

Synthesis and characterization of compounds.

Compound 3 and Compound 4 were synthesized according to the methods described below.

All reactions were carried out under a normal atmosphere and were stirred with a magnetic stirrer unless otherwise stated. All reagents were obtained from commercial sources and were used without further purification. Anhydrous solvents were dried by passing through aluminium oxide.

Analytical thin-layer chromatography (TLC) was performed on aluminium pre-coated silica gel plates (254 µm) supplied by Merck chemicals and visualised by ultraviolet light (254 nm). Preparative flash column chromatography was carried out using Thomson Single Step pre-packed silica cartridges (4-25 g) on a Biotage Isolera Flash Purification system, or dry flash vacuum chromatography using 43-65 µm silica. High-resolution mass spectrometry was carried out using a VG Autospec mass spectrometer, operating at 70 eV, using electron spray ionisation (ES+), correct to four decimal places. Analytical high performance liquid chromatography (HPLC) was performed on an Agilent 1290 Inifinity Series equipped with a UV detector and Hyperprep C-18 column with a gradient of acetonitrile and water (5-95%) and 0.1% TFA, at a flow rate of 0.5 cm^3min^{-1} over a period of five minutes.

Proton (^1H) and carbon (^{13}C) NMR spectra were recorded on a 300 / 75 MHz Bruker DPX300 or a 500 / 125 MHz Bruker Advance 500 fourier transform spectrometer as indicated. Chemical shifts (δ) are reported in parts per million (ppm) and are reported with reference to the residual solvent peak. Samples were prepared in either deuterated chloroform ($CDCl_3$) or deuterated dimethylsulfoxide (DMSO-d_6), as indicated. Multiplicities are reported with coupling constants (*J*) in Hertz and are uncorrected. Spectra were assigned with the aid of two-dimensional correlation spectroscopy (2D-COSY), performed on the same equipment as detailed above.

Infra-red spectra were recorded on a Perkin Elmer Spectrum One FT-IR spectrometer. Vibrational frequencies are reported in wavenumbers (cm^{-1}). Melting points were recorded on a Griffin melting point apparatus and are reported uncorrected.

Compound 3 was synthesized in three steps from commercially available reagents:

1-(5-Ethyl-2,4-dihydroxyphenyl)-2-(4-methoxyphenyl)ethanone

To a vessel containing 4-ethylresorcinol (2.20 g; 16.0 mmol; 1.0 eq.) and 4-methoxyphenylacetic acid (2.64 g; 16.0 mmol; 1.0 eq.) was added boron trifluoride diethyl etherate (10 mL 0.08 mol; 5.0 eq.) and resulting slurry was heated to 90°C for 2 hours with stirring, then allowed to cool. The reaction mixture was then poured slowly over sodium acetate solution (10% w/v aq.; 100 mL) and stirred for 1 hour. The resulting mixture was extracted with ethyl acetate (2x50 mL), the organics combined and then washed with water (50 mL) then with brine (50 mL), dried ($MgSO_4$) then concentrated to dryness. Purification of the residue *via* flash silica chromatography (0-15% methanol – dichloromethane) yielded the title compound as a pale orange solid (1.62 g; 5.66 mmol; 36%). **^{1}H NMR (300 MHz, DMSO-*d*$_6$):** δ 7.77 (s, 1H, C*H*CC(O)), 7.21 (d, *J* = 9.0 Hz, 2H, C*H*CHCOMe), 6.87 (d, *J* = 9.0 Hz, 2H, C*H*COMe), 6.30 (s, 1H, C(OH)C*H*C(OH)), 4.22 (s, 2H, C(O)CH_2), 3.74-3.70 (m, 4H, CH_2CH$_3$ and Both OH), 2.08 (s, 3H, OCH_3), 1.12 (t, *J* = 7.5 Hz, 3H, CH$_2$CH_3) ppm; **^{13}C NMR (75 MHz, DMSO-*d*$_6$):** δ 202.3, 162.8, 157.9, 131.7, 130.4, 127.0, 122.6, 113.7, 111.6, 102.0, 54.9, 43.2, 30.65, 22.0, 14.2 ppm; **m/z (ES+):** Found: 287.1279 $(M+H)^+$, $C_{17}H_{19}O_4$ requires 287.1279; **HPLC:** RT = 3.27 min (100%); **TLC:** R_f = 1.00 (EtOAc); **IR: ν_{max}/cm^{-1} (solid):** 3281, 2972, 1719, 1613, 1512, 1418; **M.pt:** 86-88°C.

6-Ethyl-7-hydroxy-3-(4-methoxyphenyl)-2-methyl-4H-chromen-4-one

To a slurry of 1-(5-ethyl-2,4-dihydroxyphenyl)-2-(4-methoxyphenyl)ethanone (0.7g; 2.45mmol; 1.0 eq.) and potassium carbonate (0.33g; 2.45mmol; 1.0 eq.) in *N,N*-dimethylformamide (10cm^3) was added acetic anhydride (1cm^3; 10.0mmol; 4.0 eq.) and resulting mixture was heated to 115°C with stirring for 2 hours, then allowed to cool. The reaction mixture was then poured on to water (100cm^3) and the resulting precipitate was collected *via* filtration. The solid was then washed with water (50cm^3) then with diethyl ether (2x20cm^3), yielding the title compound as an off-white solid (316mg; 1.02mmol; 42%). **^{1}H NMR (300 MHz, DMSO-*d*$_6$):** δ 7.94 (s, 1H, C*H*CC(O)), 7.17 (d, *J* = 9.0 Hz, 2H, C*H*CHCOMe), 6.98 (d, *J* = 9.0 Hz, 2H, C*H*COMe), 6.84 (s, 1H, C(OH)C*H*), 3.79 (s, 3H, OCH$_3$ H-12), 2.62 (q, *J* = 7.5 Hz, 2H, CH_2CH$_3$), 2.23 (s, 3H, CCH_3), 1.17 (t, *J* = 7.5 Hz, 3H, CH$_2$CH_3) ppm; **^{13}C NMR (75 MHz, DMSO-*d*$_6$):** δ 174.9, 162.1, 160.5, 158.4, 155.3, 131.7, 129.6, 125.5, 124.8, 121.6, 115.1, 113.4, 101.1, 79.8, 55.0, 22.3, 19.1, 13.8 ppm; **m/z (ES+):** Found: 333.1090 $(M+Na)^+$, $C_{19}H_{18}O_4Na$ requires 333.1090; **HPLC:** RT = 2.89 min (100%); **TLC:** R_f = 0.931 (EtOAc); **IR: ν_{max}/cm^{-1} (solid):** 3093, 2965, 1622, 1564, 1390; **M.pt:** >250°C.

4-Ethyl-6-(4-(4-methoxyphenyl)-3-methyl-1H-pyrazol-5-yl)benzene-1,3-diol (Compound 3)

To a solution of 6-ethyl-7-hydroxy-3-(4-methoxyphenyl)-2-methyl-4H-chromen-4-one (200mg; 0.65mmol; 1.0 eq.) in ethanol (5cm^3) was added hydrazine hydrate (0.63cm^3; 12.9mmol; 20.0 eq.) and resulting solution was heated to reflux overnight with stirring. The reaction mixture was allowed to cool, then water was added (10cm^3) and mixture was stirred for a further 15 mins. The resulting precipitate was then collected *via* filtration, yielding the title compound as an off-white powder (171mg; 0.53mmol; 82%). **^{1}H NMR (500 MHz, DMSO-d_6):** δ 7.13 (d, *J* = 9.0, 2H, C*H*CHCOMe), 6.95 (d, *J* = 9.0 Hz, 2H, C*H*COMe), 6.69 (s, 1H, CH_3CH_2CCH), 6.32 (s, 1H, C(OH)C*H*C(OH)), 3.75 (s, 3H, H-CCH_3), 3.33 (s, 3H, OCH_3), 2.18 (q, *J* = 7.5 Hz, 2H, CH_2CH$_3$), 0.78 (t, *J* = 7.5 Hz, 3H, CH$_2$CH_3) ppm; **^{13}C NMR (75 MHz, DMSO-d_6):** δ 157.9, 155.2, 154.6, 139.3, 130.9, 128.1, 126.3, 119.9, 115.9, 113.8, 108.5, 102.4, 55.0, 21.4, 13.6, 10.3 ppm; **m/z (ES+):** Found: 325.1553 $(M+H)^+$, $C_{19}H_{21}N_2O_3$ requires 325.1547; **HPLC:** RT = 2.38 min (100%); **TLC:** R_f = 0.897 (EtOAc); **IR: ν_{max}/cm^{-1} (solid):** 3384, 3331, 2961, 1612, 1519; **M.pt:** 141-143°C.

Compound 4 was synthesized in two steps from commercially available reagents:

6-Ethyl-7-hydroxy-3-(4-methoxyphenyl)-4-oxo-4H-chromene-2-carboxylic acid

A solution of 1-(5-ethyl-2,4-dihydroxyphenyl)-2-(4-methoxyphenyl)ethanone (0.5g; 1.75mmol; 1.0 eq.) in pyridine (10cm^3) was cooled to 0°C, then methyl chlorooxoacetate (1.14cm^3; 7.00mmol; 4.0 eq.) was added dropwise with stirring. Dichloromethane (20cm^3) was then added to the resulting slurry and poured on to HCl (1M aq.; 30cm^3). The organics were separated then the aqueous layer extracted with dichloromethane (2x30^3) and organics were combined, washed with brine (3x30cm^3), dried ($MgSO_4$), and concentrated to dryness to give an orange residue. This was taken up in methanol (10cm^3) and HCl (1M aq.; 10cm^3) was added and solution was heated to reflux with stirring for 4 hours. The reaction mixture was concentrated to dryness and methanol (10cm^3) and sodium bicarbonate solution (sat. aq.; 20cm^3) was added to the residue and heated to 65°C with stirring overnight. Resulting solution was allowed to cool and HCl (1M aq.) was added until solution reached pH 1 (pH paper). Resulting precipitate was collected *via* filtration and washed with a little water, then a little diethyl ether to give the title compound as an off-white powder (127mg; 0.37mmol; 21%). **^{1}H NMR (500 MHz, DMSO-d_6):** δ 7.75 (s, 1H, C*H*CC(O)), 7.26 (d, *J* = 8.5 Hz, 2H, CH_2CH$_2$OMe), 6.94 (d, *J* = 8.5 Hz, 2H, C*H*COMe), 6.91 (s, 1H, C(OH)C*H*), 3.77 (s, 3H, OCH_3), 2.62 (q, *J* = 7.5, 2H, CH_2CH$_3$), 1.17 (t, *J* = 7.5 Hz, 3H, CH$_2$CH_3) ppm; **^{13}C NMR (75 MHz, DMSO-d_6):** δ 175.5, 162.7, 161.3, 158.9, 155.0, 131.2, 130.6, 124.8, 124.0, 115.5, 113.2, 101.4, 55.0, 22.3, 13.7 ppm; **m/z (ES+):** Found: 341.1010 $(M+H)^+$, $C_{19}H_{17}O_6$ requires 341.1020; **HPLC:** RT =

2.42 min (100%); **TLC:** R_f = 0.103 (EtOAc); **IR: ν_{max}/cm^{-1} (solid):** 3134, 1728, 1573, 1513, 1412; **M.pt:** >250°C.

3-(5-Ethyl-2,4-dihydroxyphenyl)-4-(4-methoxyphenyl)-1H-pyrazole-5-carboxylic acid (Compound 4)

To a solution of 6-ethyl-7-hydroxy-3-(4-methoxyphenyl)-4-oxo-4H-chromene-2-carboxylic acid (100mg; 0.29mmol; 1.0 eq.) in ethanol (5cm^3) was added hydrazine hydrate (0.03cm^3; 0.59mmol; 2.0 eq.) and resulting mixture was heated to reflux with stirring overnight. The reaction mixture was allowed to cool and poured on to HCl (1M aq.; 20cm^3), then resulting mixture was extracted with diethyl ether (3x20cm^3). The organics were combined and washed with HCl (1M aq.; 40cm^3), dried ($MgSO_4$) and concentrated to dryness, yielding the title compound as a yellow foam (58mg; 0.164mmol; 56%). **^{1}H NMR (300 MHz, DMSO-d_6):** δ 9.58 (s, 1H, CO_2H), 9.31 (s, 1H, pyrazole N*H*), 7.12 (d, *J* = 9.0 Hz, 2H, C*H*CHCOMe), 6.84 (d, *J* = 9.0 Hz, 2H, C*H*COMe), 6.56 (s, 1H, CH_3CH_2CCH), 6.37 (s, 1H, C(OH)C*H*C(OH)), 3.73 (s, 3H, OCH_3), 2.24 (q, *J* = 7.5 Hz, 2H, CH_2CH_3), 0.85 (t, *J* = 7.5 Hz, 3H, CH_2CH_3) ppm; **^{13}C NMR (75 MHz, DMSO-d_6):** δ 174.7, 137.6, 125.9, 125.1, 123.9, 123.6, 122.8, 121.5, 119.2, 117.3, 116.9, 104.7, 19.30, 43.1, 32.1, 30.4, ppm; **m/z (ES+):** Found: 355.1294 $(M+H)^+$, $C_{19}H_{19}N_2O_5$ requires 355.1294; **HPLC:** RT = 2.23 min (100%); **TLC:** R_f = 0.207 (EtOAc); **IR: ν_{max}/cm^{-1} (solid):** 3283, 2964, 1702, 1613, 1513, 1460; **M.pt:** 214-216°C.

CCT018159, Compound 1 and 2 were purchased from commercial vendors (C2 from Tocris and Compound 1 and 2 from Enamine).

References

1. Gilden, D.H., Mahalingam, R., Cohrs, R.J. & Tyler, K.L. Herpesvirus infections of the nervous system. *Nat Clin Pract Neuro* **3**, 82-94 (2007).
2. Owen, C.B. et al. Utilising proteomic approaches to understand oncogenic human herpesviruses (Review). *Molecular and Clinical Oncology* **2**, 891-903 (2014).
3. Quadrelli, C. et al. β-HHVs and HHV-8 in Lymphoproliferative Disorders. *Mediterranean Journal of Hematology and Infectious Diseases* **3**, e2011043 (2011).
4. Ganem, D. KSHV infection and the pathogenesis of Kaposi's sarcoma. *Annu Rev Pathol* **1**, 273-296 (2006).
5. Mesri, E.A., Cesarman, E. & Boshoff, C. Kaposi's sarcoma and its associated herpesvirus. *Nat. Rev. Cancer* **10**, 707-719 (2010).
6. Arvanitakis, L., GerasRaaka, E., Varma, A., Gershengorn, M.C. & Cesarman, E. Human herpesvirus KSHV encodes a constitutively active G-protein-coupled receptor linked to cell proliferation. *Nature* **385**, 347-350 (1997).
7. Vart, R.J. et al. Kaposi's Sarcoma–Associated Herpesvirus-Encoded Interleukin-6 and G-Protein–Coupled Receptor Regulate Angiopoietin-2 Expression in Lymphatic Endothelial Cells. *Cancer Research* **67**, 4042-4051 (2007).
8. Nicholas, J. et al. Kaposi's sarcoma-associated human herpesvirus-8 encodes homologues of macrophage inflammatory protein-1 and interleukin-6. *Nature Medicine* **3**, 287-292 (1997).
9. Tomlinson, C.C. & Damania, B. The K1 Protein of Kaposi's Sarcoma-Associated Herpesvirus Activates the Akt Signaling Pathway. *Journal of Virology* **78**, 1918-1927 (2004).
10. Brinkmann, M.M. et al. Activation of Mitogen-Activated Protein Kinase and NF-κB Pathways by a Kaposi's Sarcoma-Associated Herpesvirus K15 Membrane Protein. *Journal of Virology* **77**, 9346-9358 (2003).
11. Jackson, B.R., Noerenberg, M. & Whitehouse, A. A novel mechanism inducing genome instability in Kaposi's sarcoma-associated herpesvirus infected cells. *PLoS Pathogens* **10**(2014).
12. Bacon, T.H., Levin, M.J., Leary, J.J., Sarisky, R.T. & Sutton, D. Herpes simplex virus resistance to acyclovir and penciclovir after two decades of antiviral therapy. *Clinical Microbiology Reviews* **16**, 114-128 (2003).
13. Fife, K. et al. Cidofovir for the treatment of Kaposi's sarcoma in an HIV-negative homosexual man. *British Journal of Dermatology* **141**, 1148-1150 (1999).
14. Mazzi, R. et al. Efficacy of cidofovir on human herpesvirus 8 viraemia and Kaposi's sarcoma progression in two patients with AIDS. *AIDS* **15**, 2061-2062 (2001).
15. Little, R.F. et al. A pilot study of cidofovir in patients with Kaposi sarcoma. *Journal of Infectious Diseases* **187**, 149-153 (2003).
16. Martin, D.F. et al. Oral ganciclovir for patients with cytomegalovirus retinitis treated with a ganciclovir implant. *New England Journal of Medicine* **340**, 1063-1070 (1999).
17. Glesby, M.J. et al. Use of Antiherpes Drugs and the Risk of Kaposi's Sarcoma: Data from the Multicenter AIDS Cohort Study. *Journal of Infectious Diseases* **173**, 1477-1480 (1996).

735 18. Cordin, O., Banroques, J., Tanner, N.K. & Linder, P. The DEAD-box protein
736 family of RNA helicases. *Gene* **367**, 17-37 (2006).
737 19. Shadrick, W.R. et al. Discovering New Medicines Targeting Helicases:
738 Challenges and Recent Progress. *Journal of Biomolecular Screening* **18**, 761-
739 781 (2013).
740 20. Chen, C.-S. et al. Structure-Based Discovery of Triphenylmethane Derivatives
741 as Inhibitors of Hepatitis C Virus Helicase∞. *Journal of Medicinal Chemistry* **52**,
742 2716-2723 (2009).
743 21. Artsaenko, O., Tessmann, K., Sack, M., Häussinger, D. & Heintges, T.
744 Abrogation of hepatitis C virus NS3 helicase enzymatic activity by recombinant
745 human antibodies. *Journal of General Virology* **84**, 2323-2332 (2003).
746 22. Hwang, B. et al. Isolation of specific and high-affinity RNA aptamers against
747 NS3 helicase domain of hepatitis C virus. *RNA* **10**, 1277-1290 (2004).
748 23. Lindqvist, L. et al. Selective Pharmacological Targeting of a DEAD Box RNA
749 Helicase. *PLoS ONE* **3**, e1583 (2008).
750 24. Tsumuraya, T. et al. Effects of hippuristanol, an inhibitor of eIF4A, on adult T-
751 cell leukemia. *Biochemical Pharmacology* **81**, 713-722 (2011).
752 25. Yedavalli, V.S.R.K. et al. Ring expanded nucleoside analogues inhibit RNA
753 helicase and intracellular human immunodeficiency virus type 1 replication.
754 *Journal of Medicinal Chemistry* **51**, 5043-5051 (2008).
755 26. Boyne, J.R. & Whitehouse, A. gamma-2 Herpes virus post-transcriptional gene
756 regulation. *Clin Microbiol Infect* **12**, 110-7 (2006).
757 27. Schumann, S., Jackson, B., Baquero-Perez, B. & Whitehouse, A. Kaposi's
758 sarcoma-associated herpesvirus ORF57 protein: exploiting all stages of viral
759 mRNA processing. *Viruses* **5**, 1901-1923 (2013).
760 28. Boyne, J.R., Jackson, B.R., Taylor, A., Macnab, S.A. & Whitehouse, A. Kaposi's
761 sarcoma-associated herpesvirus ORF57 protein interacts with PYM to enhance
762 translation of viral intronless mRNAs. *Embo J* **29**, 1851-1864 (2010).
763 29. Jackson, B.R. et al. An interaction between KSHV ORF57 and UIF provides
764 mRNA-adaptor redundancy in herpesvirus intronless mRNA export. *PLoS*
765 *Pathog* **7**, e1002138 (2011).
766 30. Hautbergue, G.M. et al. UIF, a new mRNA export adaptor that works together
767 with REF/ALY, requires FACT for recruitment to mRNA. *Curr Biol* **19**, 1918-
768 1924 (2009).
769 31. Dufu, K. et al. ATP is required for interactions between UAP56 and two
770 conserved mRNA export proteins, Aly and CIP29, to assemble the TREX
771 complex. *Genes Dev* **24**, 2043-2053 (2010).
772 32. Chang, C.T. et al. Chtop is a component of the dynamic TREX mRNA export
773 complex. *EMBO J* **32**, 473-486 (2013).
774 33. Boyne, J.R., Colgan, K.J. & Whitehouse, A. Recruitment of the complete
775 hTREX complex is required for Kaposi's sarcoma-associated herpesvirus
776 intronless mRNA nuclear export and virus replication. *PLoS Pathog* **4**,
777 e1000194 (2008).
778 34. Shi, H., Cordin, O., Minder, C.M., Linder, P. & Xu, R.-M. Crystal structure of the
779 human ATP-dependent splicing and export factor UAP56. *Proceedings of the*
780 *National Academy of Sciences of the United States of America* **101**, 17628-
781 17633 (2004).
782 35. Dymock, B.W. et al. Novel, potent small-molecule inhibitors of the molecular
783 chaperone Hsp90 discovered through structure-based design. *Journal of*
784 *Medicinal Chemistry* **48**, 4212-4215 (2005).

785 36. Shen, J., Zhang, L. & Zhao, R. Biochemical characterization of the ATPase and
786 helicase activity of UAP56, an essential pre-mRNA splicing and mRNA export
787 factor. *Journal of Biological Chemistry* **282**, 22544-22550 (2007).
788 37. Sharp, S.Y. et al. In vitro biological characterization of a novel, synthetic diaryl
789 pyrazole resorcinol class of heat shock protein 90 inhibitors. *Cancer Research*
790 **67**, 2206-2216 (2007).
791 38. Boyne, J.R. & Whitehouse, A. Nucleolar disruption impairs Kaposi's sarcoma-
792 associated herpesvirus ORF57-mediated nuclear export of intronless viral
793 mRNAs. *FEBS Lett* **583**, 3549-3556 (2009).
794 39. Schumann, S., Baquero-Perez, B. & Whitehouse, A. Interactions between
795 KSHV ORF57 and the novel human TREX proteins, CHTOP and CIP29.
796 *Journal of General Virology* **97**, 1904-1910 (2016).
797 40. Stubbs, S.H., Hunter, O.V., Hoover, A. & Conrad, N.K. Viral factors reveal a
798 role for REF/Aly in nuclear RNA stability. *Molecular and Cellular Biology* **32**,
799 1260-1270 (2012).
800 41. Nakamura, H. et al. Global changes in Kaposi's sarcoma-associated virus gene
801 expression patterns following expression of a tetracycline-inducible Rta
802 transactivator. *Journal of Virology* **77**, 4205-4220 (2003).
803 42. Chen, W., Sin, S.-H., Wen, K.W., Damania, B. & Dittmer, D.P. Hsp90 inhibitors
804 are efficacious against Kaposi Sarcoma by enhancing the degradation of the
805 essential viral gene LANA, of the viral co-receptor EphA2 as well as other client
806 proteins. *PLoS Pathogens* **8**(2012).
807 43. Nayar, U. et al. Targeting the Hsp90-associated viral oncoproteome in
808 gammaherpesvirus-associated malignancies. *Blood* **122**, 2837-2847 (2013).
809 44. Higashi, C. et al. The Effects of Heat Shock Protein 90 Inhibitors on Apoptosis
810 and Viral Replication in Primary Effusion Lymphoma Cells. *Biological and*
811 *Pharmaceutical Bulletin* **35**, 725-730 (2012).
812 45. Zhao, R., Shen, J., Green, M.R., MacMorris, M. & Blumenthal, T. Crystal
813 structure of UAP56, a DExD/H-box protein involved in pre-mRNA splicing and
814 mRNA export. *Structure* **12**, 1373-1381 (2004).
815 46. Nielsen, K.H. et al. Mechanism of ATP turnover inhibition in the EJC. *RNA* **15**,
816 67-75 (2009).
817 47. Smith, N.F. et al. Preclinical pharmacokinetics and metabolism of a novel diaryl
818 pyrazole resorcinol series of heat shock protein 90 inhibitors. *Molecular Cancer*
819 *Therapeutics* **5**, 1628-1637 (2006).
820 48. Tunnicliffe, R.B. et al. Structural basis for the recognition of cellular mRNA
821 export factor REF by herpes viral proteins HSV-1 ICP27 and HVS ORF57.
822 *PLoS Pathog* **7**, e1001244 (2011).
823 49. Lischka, P., Toth, Z., Thomas, M., Mueller, R. & Stamminger, T. The UL69
824 transactivator protein of human cytomegalovirus interacts with DEXD/H-box
825 RNA helicase UAP56 to promote cytoplasmic accumulation of unspliced RNA.
826 *Molecular and Cellular Biology* **26**, 1631-1643 (2006).
827 50. Read, E.K.C. & Digard, P. Individual influenza A virus mRNAs show differential
828 dependence on cellular NXF1/TAP for their nuclear export. *Journal of General*
829 *Virology* **91**, 1290-1301 (2010).
830 51. http://zinc.docking.org/.
831 52. Cheng, H. et al. Human mRNA export machinery recruited to the 5' end of
832 mRNA. *Cell* **127**, 1389-1400 (2006).
833 53. Hughes, D.J., Wood, J.J., Jackson, B.R., Baquero-Pérez, B. & Whitehouse, A.
834 NEDDylation Is Essential for Kaposi's Sarcoma-Associated Herpesvirus

Latency and Lytic Reactivation and Represents a Novel Anti-KSHV Target. *PLoS Pathogens* **11**, e1004771 (2015).
54. Griffiths, D.A. et al. Merkel Cell Polyomavirus Small T Antigen Targets the NEMO Adaptor Protein To Disrupt Inflammatory Signaling. *Journal of Virology* **87**, 13853-13867 (2013).
55. Knight, L.M. et al. Merkel cell polyomavirus small T antigen mediates microtubule destabilisation to promote cell motility and migration. *Journal of Virology* (2014).

Figure Legends

Figure 1: ATP-cycle dependent remodeling of hTREX affects ORF57-mediated vRNP formation. (**a**) Immunoprecipitations of GFP or GFP-UAP56, co-expressed in the absence or presence of mCherry-ORF57. Precipitations were performed with HEK-293T whole cell lysates (Input) in the absence of any additional nucleotides or in presence of 1.25 mM ATP or 1.25 mM ATPγS. Samples were analyzed by western blotting using the indicated antibodies. (**b**) Quantification of 4 independent immunoprecipitations (performed with mCherry-ORF57, as shown in **a**, or Myc-ORF57). Values are averages, error bars present SD, n = 4. $p < 0.01$ (**) or $p < 0.05$ (*), effect of ATP or ATPγS compared to untreated, using an unpaired *t* test. (**c**) Immunoprecipitations of GFP-UAP56 after co-expression with mCherry-ORF57. Precipitations were performed with HEK-293T whole cell lysate (Input) in the absence of any additional nucleotides or with increasing concentrations of nucleotides, as indicated. Samples were analyzed by western blotting using the indicated antibodies. (**d**) Quantification of 3 independent immunoprecipitations (at concentrations of 1.25 or 1.75 mM ATP, ATPγS or ADP). Values are averages, error bars present SD, n = 3. $p < 0.05$ (*), $p < 0.01$ (**) or $p < 0.001$ (***) effect of ATP or ATPγS compared to untreated, using an unpaired *t* test. (**e**) Schematic representation of ATP-cycle dependent remodeling of central hTREX components and the ORF57-mediated vRNP. The proposed model is based on the immunoprecipitations shown in **a-d**.

Figure 2: Identification of UAP56-targeted ATPase inhibitor. (**a**) Chemical structure of UAP56 ATPase inhibitor CCT018159, identified through *in silico* high-throughput and *in vitro*

867 screening against UAP56 ATPase activity. (**b**) Predicted binding mode of CCT018159 (orange
868 sticks) to the ATP-binding pocket of UAP56. Docking routine performed using AutoDock4
869 (Scripps Research Institute) and the UAP56Δ9 MgADP complex (PDB ID: 1XTJ). Polar
870 interactions are shown as dotted lines. (**c**) Surface potential representation of **b**, showing the
871 occupancy of the AT(D)P binding site by CCT018159 by overlay with ADP (purple lines) from
872 the co-crystallised UAP56:ADP structure. Docking routine performed using AutoDock4
873 (Scripps Research Institute) and the UAP56Δ9 MgADP complex (PDB ID: 1XTJ). (**d**) 2-
874 dimensional representation of CCT018159 in the UAP56 binding site. All key interacting
875 residues are highlighted and hydrogen bonds are shown as dashed lines and a π-stack
876 interaction as waves. (**e**) IC_{50} of CCT018159 for UAP56 ATP-hydrolysis. *In vitro* ATPase
877 activity of purified recombinant UAP56 was measured in the presence of increasing
878 concentrations of CCT018159. Values are averages from 7 assays performed after
879 independent protein purification processes of recombinant protein, n = 21, error bars display
880 the SD. The IC_{50} was determined using non-linear regression with a variable slope (four-
881 parameter logistic curve). (**f**) Microscale thermophoresis binding curves for binding of
882 CCT018159 and ATP to UAP56. Data are plotted for normalized signal change as a function
883 of CCT018159 or ATP concentration, respectively. Values are averages, error bars present
884 the SD, n = 3. (**g**) ADP-displacement from UAP56 by CCT018159. Free ADP was measured
885 after increasing concentrations of CCT018159 were added to ADP-bound purified
886 recombinant UAP56. Values are averages, error bars present SD, n = 3.
887
888 **Figure 3: CCT018159 disrupts formation and function of the vRNP, but not of the**
889 **endogenous hTREX complex.** (**a**) Cell viability of HEK-293T cells in the presence of
890 increasing amounts of CCT018159 as measured by MTS assay. Data was normalized to
891 DMSO treated control cells. Values are averages, n = 5, error bars display SD. The CC_{50} was
892 determined using non-linear regression with a variable slope (four-parameter logistic curve).
893 (**b**) Immunoprecipitations of endogenous UAP56 in GFP or ORF57-GFP expressing cells.
894 HEK-293T cells were treated with indicated amounts of CCT018159 6 h after transfection.

Precipitations were performed with whole cell lysates (Input) in the absence or in presence of the indicated CCT018159 concentration range or DMSO control. Samples were analyzed by western blotting using the indicated antibodies. Results are representative of 3 independent repeats at varying concentrations. (**c**) HEK-293T cells co-expressing GFP or ORF57-GFP and the intronless reporter construct ORF47 were treated with DMSO or 2.5 µM CCT018159. qRT-PCR was performed after subcellular fractionation. ORF47 transcript levels were normalized to GAPDH and the relative increase calculated using the ΔΔCT method. Values are averages, n = 3, error bars display SD, $p < 0.05$ (*) or $p < 0.001$ (***), effect CCT018159 compared to DMSO treated, using an unpaired *t* test. (**d**) HEK-293T cells expressing GFP or ORF57-GFP were treated with DMSO or 2.5 µM CCT018159, as indicated. A fluorescently labelled oligo(dT) probe was used to detect poly(A) RNA, DAPI visualizes the nucleus. Arrows indicate localization of poly(A) RNA. Scale bar = 20 µm. Images representative of 4 independent experiments. (**e**) Quantification of cells with nuclear mRNA retention in GFP or ORF57-GFP transfected cells, treated with DMSO or CCT018159, as indicated. Values are averages of 4 independent experiments (GFP + DMSO and ORF57-GFP + CCT018159) or 6 independent experiments (ORF57-GFP + DMSO), error bars present the SD. A total of 32 GFP transfected and 76 ORF57-GFP transfected cells (for each treatment) were counted. $p < 0.001$, effect of DMSO compared to CCT018159 treated, using a Fisher's exact test.

Figure 4: Disruption of virus lytic replication and infectious virion production by CCT018159. (**a**, **b**) Viability of TREx BCBL1-Rta cells in the presence of CCT018159 at 24 and 72 h, determined by MTS assay. (**c**) Expression of viral late protein mCP in TREx BCBL1-Rta cells after normalization to GAPDH, as determined by western blotting using mCP- and GAPDH-specific antibodies. Cell viability values from **a** are shown in comparison. (**d**) Viral load in TREx BCBL1-Rta cells in response to CCT018159 was measured by qPCR, 72 h after induction of KSHV lytic replication. Viral DNA was normalized to GAPDH and the relative decrease compared to DMSO treated samples calculated using the ΔΔCT method. Cell viability values from **b** are shown in comparison. (**e**) Production of infectious KSHV virions was

923 determined by re-infection of HEK-293T cells, 72 h after induction of lytic replication in TREx
924 BCBL1-Rta cells and treatment with 2.5 µM CCT018159. Viral mRNA levels were determined
925 by qRT-PCR and normalized to GAPDH, and are shown as fold change compared to DMSO
926 treated controls. $p < 0.01$ using an unpaired *t* test. For all figures: Values are averages, error
927 bars present SD. EC_{50} and CC_{50} values were determined using non-linear regression with a
928 variable slope (four-parameter logistic curve). (**a**, **b**) n = 5, (**c**, **d**) n = 4, (**e**) n = 6.
929
930 **Table 1: Close structural analogues of CCT018159 and their effect on UAP56 ATPase**
931 **activity, cell viability and KSHV lytic replication.** The schematic shows the common
932 structure of CCT018159 and its close structural analogues. Functional groups that differ
933 between the analogues are indicated, as well as the effect of these changes on ATPase
934 activity of purified UAP56, cell viability at 24 and 72 h, viral late protein expression and viral
935 load of TREx BCBL1-Rta cells. Values are mean ± s.e.m, n ≥ 3 for all experiments. *Due to
936 minimal effect of Compound 4 in most biological assays, not all data points were found to
937 converge or present a trend that could be displayed by nonlinear regression. IC_{50}, CC_{50} and
938 EC_{50} values outside of the tested range had to be extrapolated from the obtained data.
939
940 **Figure 5: Inhibition of α- and β-herpesvirus replication by CCT018159.** (**a, b**)
941 Immunoprecipitations of endogenous UAP56 in (**a**) GFP and ICP27-GFP or (**b**) GFP and
942 UL69-GFP expressing cells. HEK-293T cells were treated with indicated amounts of
943 CCT018159, 6 h after transfection. Precipitations were performed with whole cell lysates
944 (Input) in the absence or in presence of the indicated CCT018159 concentration range or
945 DMSO control. Samples were analyzed by western blotting using the indicated antibodies.
946 Results are representative of 3 independent repeats at varying concentrations. (**c, d**) Viability
947 of HFF cells in the presence of CCT018159 at 72 and 168 h, determined by MTS assay.
948 Values are averages, error bars present SD, n = 5. CC_{50} values were determined using non-
949 linear regression with a variable slope (four-parameter logistic curve). (**e**) Plaque assay in the
950 absence or presence of increasing amounts of CCT018159, 120 h after primary infection with

HSV-1. Scale bar = 2 cm. Results are representative of 2 independent repeats. (**f**) Production of infectious HSV-1 virions was measured by re-infection of HFF cells, 72 h after primary infection and treatment with CCT018159. Supernatants of primary infected cells were diluted 1:100 before being added to fresh HFF cells. The percentage of infected cells was determined by flow cytometry, assessing ≥ 10,000 cells. (**g**) HSV-1 infectious virion production was also assessed by plaque assay. Virion containing supernatants were used to reinfect HFF cells, 72 h after primary infection and treatment with CCT018159. Plaques were counted 120 h after re-infection. Values are averages, error bars present SD, n = 4. (**h**) HCMV infectious virion production was assessed by re-infection assay, 168 h after initial infection of HFF cells and treatment with CCT018159. Levels of re-infection were determined by qPCR, with viral DNA levels normalized to GAPDH. The percentage of infected cells is shown relative to DMSO treated control cells. Values are averages, error bars present SD, n = 3.

Figure 1

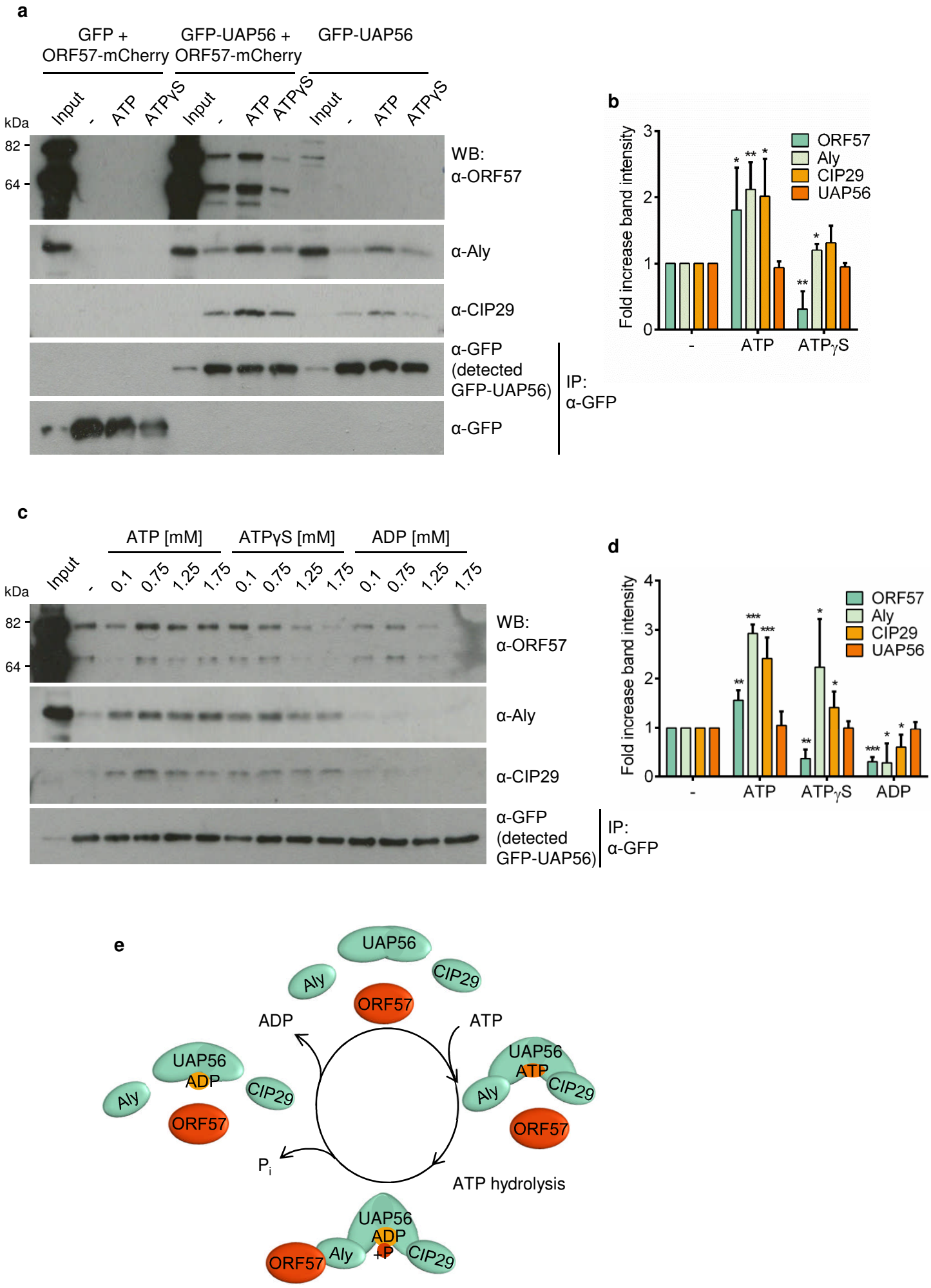
a
GFP + ORF57-mCherry
GFP-UAP56 + ORF57-mCherry
GFP-UAP56
Input
-
ATP
ATPγS
kDa
82
64
WB: α-ORF57
α-Aly
α-CIP29
α-GFP (detected GFP-UAP56)
α-GFP
IP: α-GFP
b
Fold increase band intensity
ORF57
Aly
CIP29
UAP56
-
ATP
ATPγS
c
ATP [mM]
ATPγS [mM]
ADP [mM]
0.1
0.75
1.25
1.75
d
ADP
e
UAP56
Aly
CIP29
ORF57
ATP
UAP56 ADP
UAP56 ATP
Pi
ATP hydrolysis
+P

Figure 2

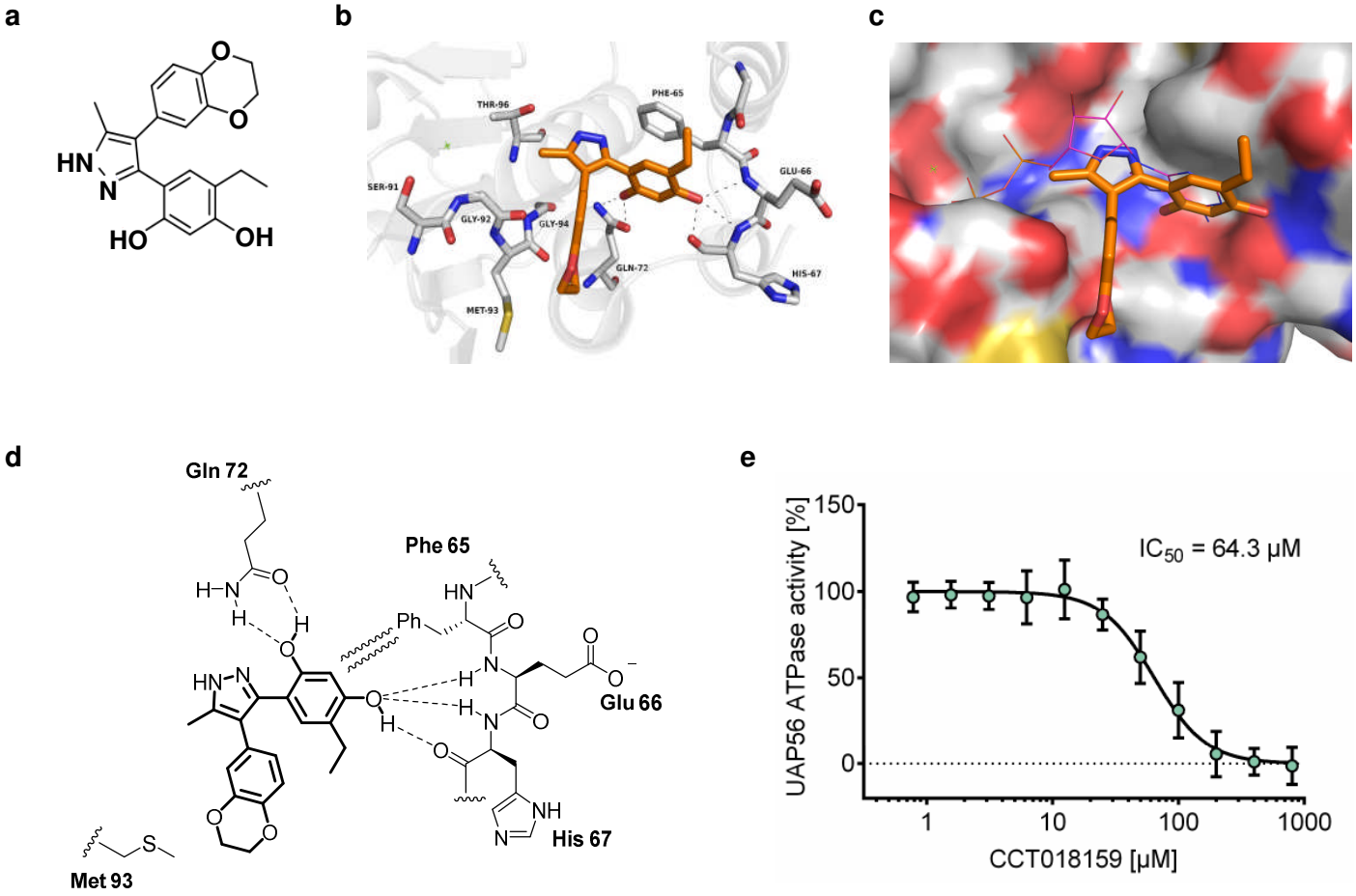
a
b
c
d
e
f
g
THR-96
PHE-65
SER-91
GLU-66
GLY-92
GLY-94
GLN-72
HIS-67
MET-93
Gln 72
Phe 65
Glu 66
His 67
Met 93
UAP56 ATPase activity [%]
IC50 = 64.3 µM
CCT018159 [µM]
Normalized signal
ATP
CCT018159
Ligand concentration [µM]
Displacement of ADP [%]
CCT018159 [µM]

Figure 3

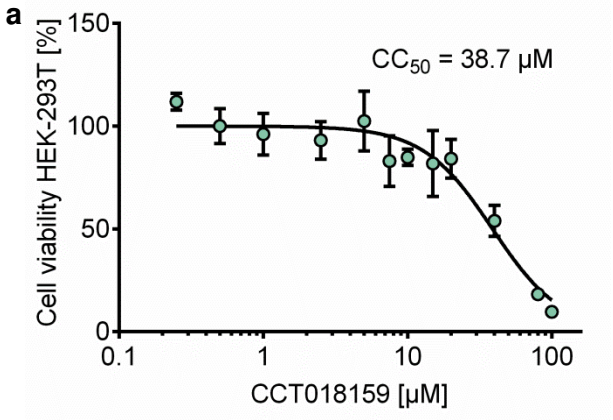
a
Cell viability HEK-293T [%]
150
100
50
0
0.1
1
10
100
CCT018159 [μM]
CC50 = 38.7 μM

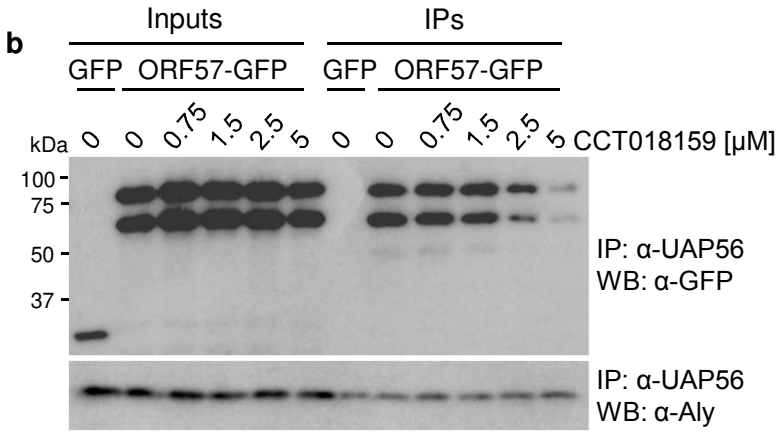
b
Inputs
IPs
GFP
ORF57-GFP
GFP
ORF57-GFP
kDa
0
0
0.75
1.5
2.5
5
0
0
0.75
1.5
2.5
5
CCT018159 [μM]
100
75
50
37
IP: α-UAP56
WB: α-GFP
IP: α-UAP56
WB: α-Aly

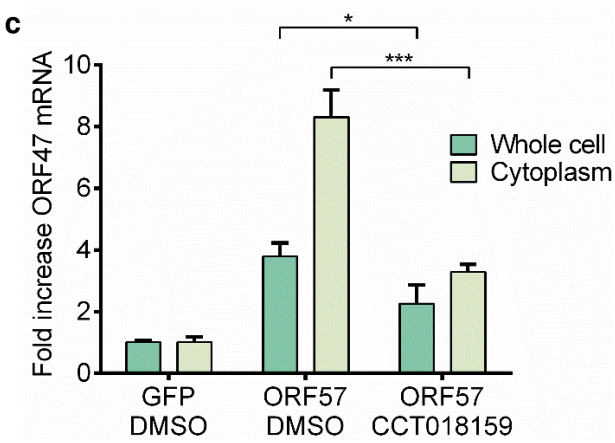
c
Fold increase ORF47 mRNA
10
8
6
4
2
0
*
***
Whole cell
Cytoplasm
GFP
DMSO
ORF57
DMSO
ORF57
CCT018159

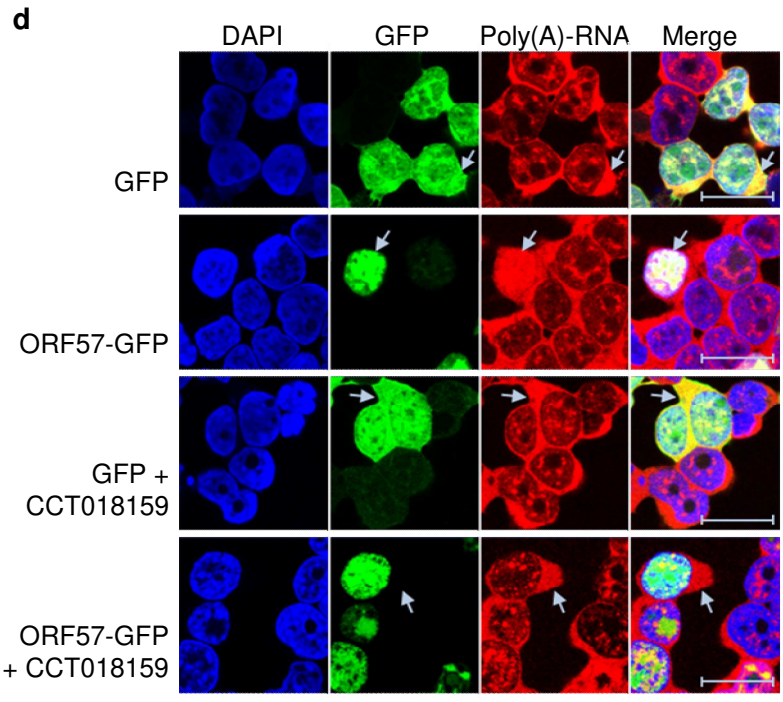
d
DAPI
GFP
Poly(A)-RNA
Merge
GFP
ORF57-GFP
GFP +
CCT018159
ORF57-GFP
+ CCT018159

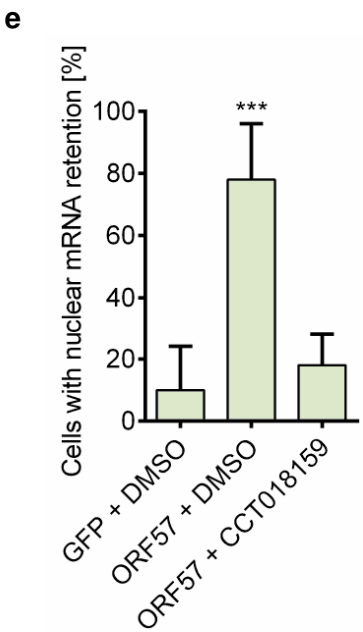
e
Cells with nuclear mRNA retention [%]
100
80
60
40
20
0
***
GFP + DMSO
ORF57 + DMSO
ORF57 + CCT018159

Figure 4

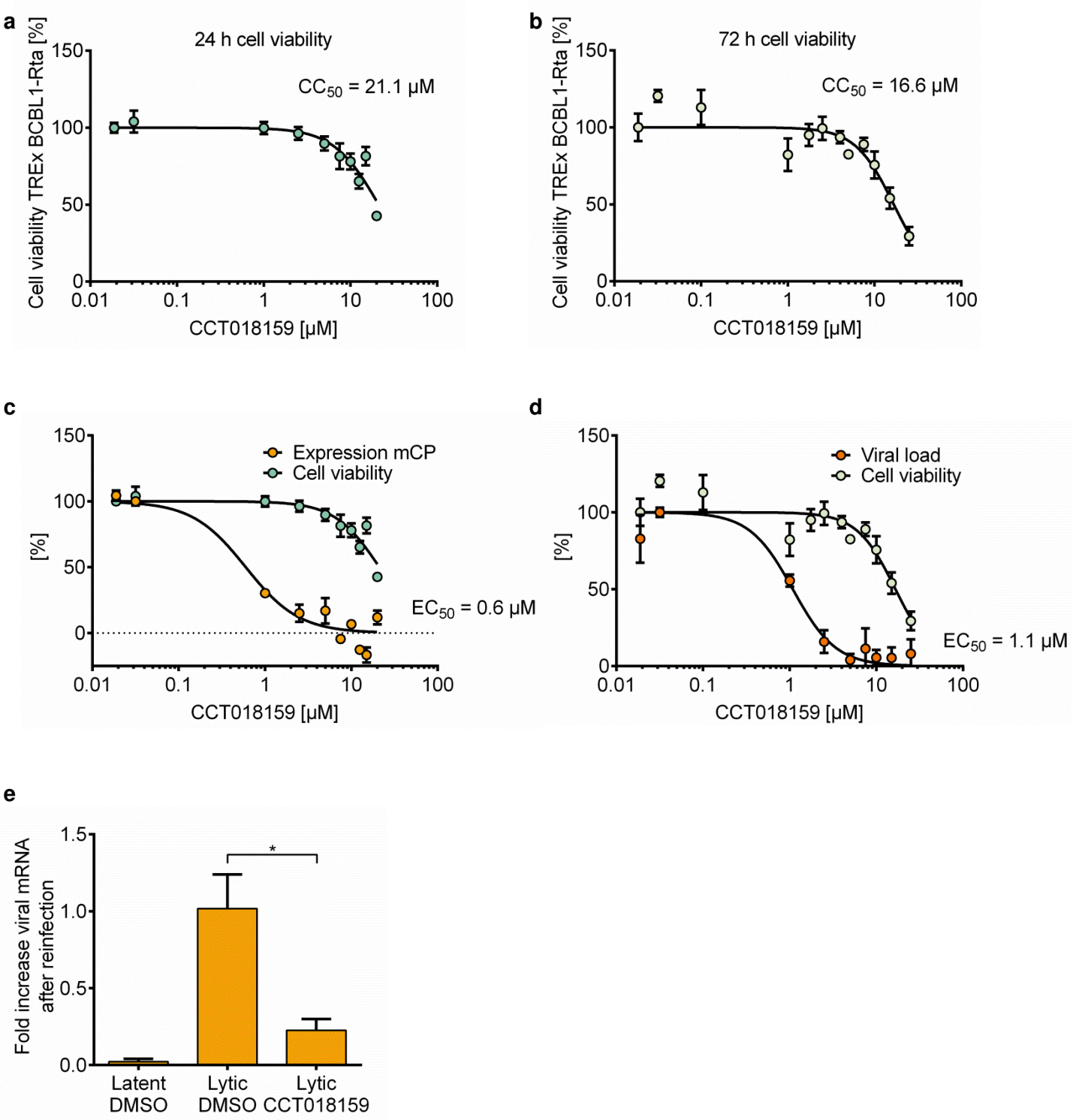
a
24 h cell viability
CC50 = 21.1 µM
Cell viability TREx BCBL1-Rta [%]
CCT018159 [µM]
b
72 h cell viability
CC50 = 16.6 µM
Cell viability TREx BCBL1-Rta [%]
CCT018159 [µM]
c
Expression mCP
Cell viability
EC50 = 0.6 µM
[%]
CCT018159 [µM]
d
Viral load
Cell viability
EC50 = 1.1 µM
[%]
CCT018159 [µM]
e
Fold increase viral mRNA after reinfection
*
Latent DMSO
Lytic DMSO
Lytic CCT018159

Table 1

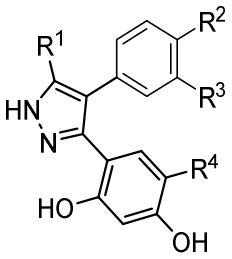

Cmpd.	R1	R2	R3	R4	IC_{50} (μM) (ATPase assay)	CC_{50} 24 h (μM) (Cell viability)	CC_{50} 72 h (μM) (Cell viability)	EC_{50} 24 h (μM) (mCP expression)	EC_{50} 72 h (μM) (Viral load)
CCT018159	Me	-OCH_2CH_2O-		Et	64.3 ± 2.5	21.1 ± 1.6	16.6 ± 1.1	0.6 ± 0.1	1.1 ± 0.1
Cmpd. 1	Me	H	H	Et	127.4 ± 8.4	28.9 ± 1.7	7.6 ± 0.1	3.1 ± 0.2	1.5 ± 0.1
Cmpd. 2	Me	-OCH_2CH_2O-		H	309 ± 26.4	46.1 ± 3.8	25.1 ± 2.4	2.4 ± 0.3	5.1 ± 0.4
Cmpd. 3	Me	OMe	H	Et	88.7 ± 7.9	27.9 ± 2.7	14.7 ± 0.5	2.4 ± 0.4	2.7 ± 0.2
Cmpd. 4	CO_2H	OMe	H	Et	> 1000*	~ 820*	> 1000*	> 1000*	138.1 ± 45.2*

Figure 5

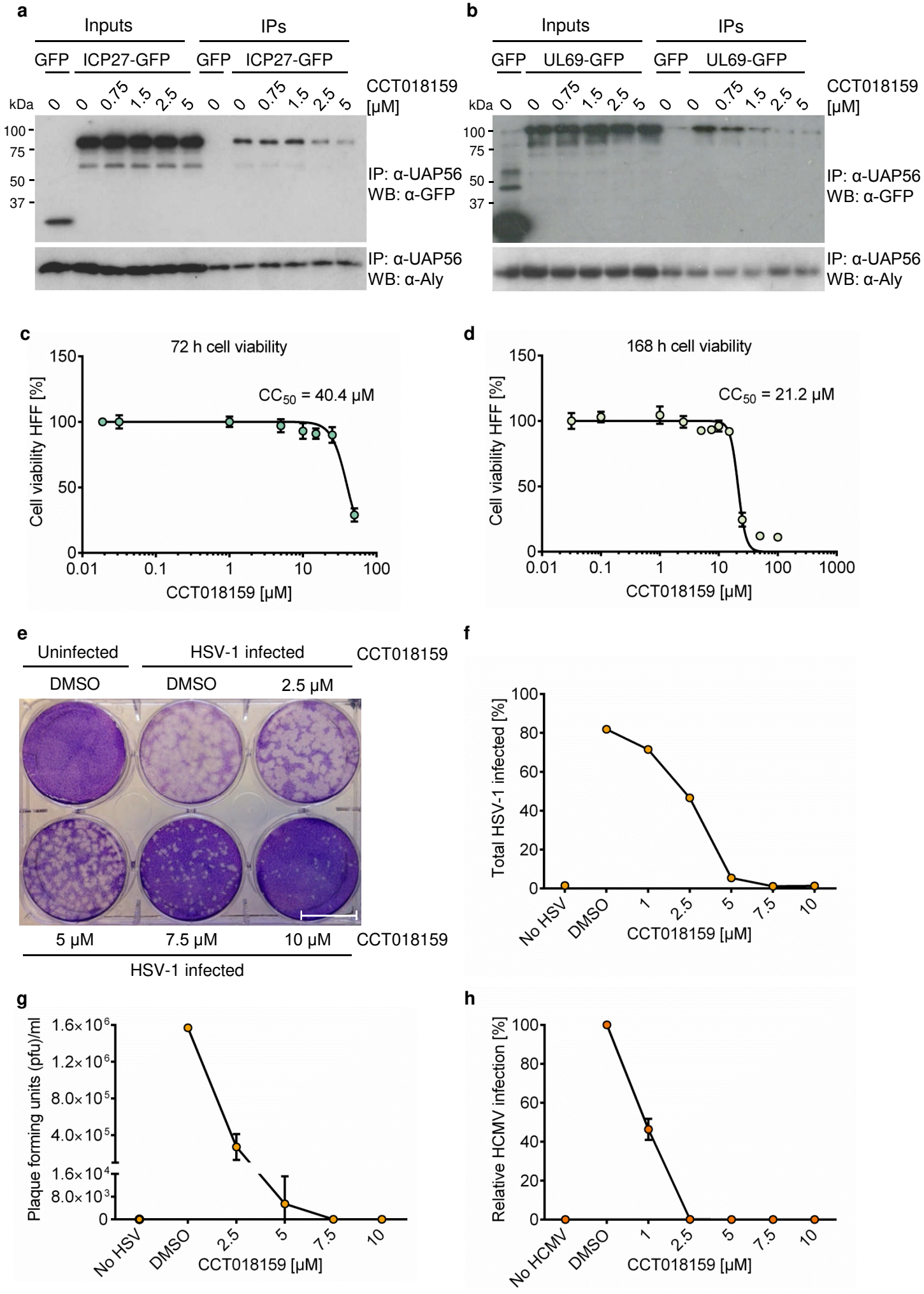
a
Inputs
IPs
GFP
ICP27-GFP
GFP
ICP27-GFP
kDa
0
0
0.75
1.5
2.5
5
0
0
0.75
1.5
2.5
5
CCT018159 [μM]
100
75
50
37
IP: α-UAP56
WB: α-GFP
IP: α-UAP56
WB: α-Aly
b
Inputs
IPs
GFP
UL69-GFP
GFP
UL69-GFP
kDa
0
0
0.75
1.5
2.5
5
0
0
0.75
1.5
2.5
5
CCT018159 [μM]
100
75
50
37
IP: α-UAP56
WB: α-GFP
IP: α-UAP56
WB: α-Aly
c
72 h cell viability
CC50 = 40.4 μM
Cell viability HFF [%]
150
100
50
0
0.01
0.1
1
10
100
CCT018159 [μM]
d
168 h cell viability
CC50 = 21.2 μM
Cell viability HFF [%]
150
100
50
0
0.01
0.1
1
10
100
1000
CCT018159 [μM]
e
Uninfected
HSV-1 infected
CCT018159
DMSO
DMSO
2.5 μM
5 μM
7.5 μM
10 μM
CCT018159
HSV-1 infected
f
Total HSV-1 infected [%]
100
80
60
40
20
0
No HSV
DMSO
1
2.5
5
7.5
10
CCT018159 [μM]
g
Plaque forming units (pfu)/ml
1.6×10^6
1.2×10^6
8.0×10^5
4.0×10^5
1.6×10^4
8.0×10^3
0
No HSV
DMSO
2.5
5
7.5
10
CCT018159 [μM]
h
Relative HCMV infection [%]
100
80
60
40
20
0
No HCMV
DMSO
1
2.5
5
7.5
10
CCT018159 [μM]